Research Square

Preprints are preliminary reports that have not undergone peer review.
They should not be considered conclusive, used to inform clinical practice,
or referenced by the media as validated information.

Immunometabolic hyperactivation of kidney-resident NK cells drives tubular injury in early diabetic nephropathy

Yu Meng

meng.yu@gzhmu.edu.cn

Department of Nephrology, The Second Affiliated Hospital of Guangzhou Medical University, Guangzhou

Xiaqing Li

The First Affiliated Hospital of Jinan University

lei luo

The First Affiliated Hospital of Jinan University

Xiayun Liu

The First Affiliated Hospital of Jinan University

Shiting Zhang

The First Affiliated Hospital of Jinan University

Ke Ma

The First Affiliated Hospital of Jinan University

Mengyun Xiao

Institute of Nephrology and Blood Purification, Jinan University, Guangzhou, Guangdong 510632, China

Huan-huan Liu

The First Affiliated Hospital of Jinan University

Hongyue Li

The First Affiliated Hospital of Jinan University

Le Li

Department of Medical Biochemistry and Molecular Biology, School of Medicine, Jinan University, Guangzhou, Guangdong 510632, China

Bo Hu

The First Affiliated Hospital of Jinan University

Lianghong Yin

The First Affiliated Hospital of Jinan University

Jun Fan

Department of Medical Biochemistry and Molecular Biology, School of Medicine, Jinan University

Article

Keywords:

Posted Date: November 20th, 2026

DOI: https://doi.org/10.21203/rs.3.rs-11417931/v1

License: This work is licensed under a Creative Commons Attribution 4.0 International License.
Read Full License

Additional Declarations: (Not answered)

Immunometabolic hyperactivation of kidney-resident NK cells drives tubular injury in early diabetic nephropathy

Xiaqing Li [1,3,#], Lei Luo [1,2,#], Xiayun Liu [1,#], Shiting Zhang [1], Ke Ma [1,2], Mengyun Xiao [1,6], Huan-huan Liu [1], Hongyue Li [1], Le Li [4,5], Bo Hu [1], Lianghong Yin [1,*], Jun Fan [4,5,*], & Yu Meng [2,*]

[1]Institute of Nephrology and Blood Purification, Jinan University, Guangzhou, Guangdong 510632, China

[2]Department of Nephrology, The Second Affiliated Hospital of Guangzhou Medical University, Guangzhou, Guangdong 510290, China

[3]Department of Nephrology, Peking University Shenzhen Hospital, Shenzhen, Guangdong 518000, China

[4]Department of Medical Biochemistry and Molecular Biology, School of Medicine, Jinan University, Guangzhou, Guangdong 510632, China

[5]Key Laboratory of Viral Pathogenesis & Infection Prevention and Control (Jinan University), Ministry of Education, Guangzhou, Guangdong 510632, China

[6]School of Medicine, Qinghai University, Xining 810016, Qinghai, China

[*]Correspondence: Yin-yun@126.com (L.H.Y.), fanjun@jnu.edu.cn (J.F.), meng.yu@gzhmu.edu.cn (Y.M.)

# These authors contributed equally to this work.

Abstract

Accumulating evidence indicates that local immunometabolic crosstalk plays a critical role in the pathogenesis of diabetic nephropathy (DN). However, the specific contribution of tissue-resident innate immunity during the early stages of the disease remains poorly understood. Here, we identify that renal tissue-resident natural killer cells (trNKs) undergo a marked early accumulation coupled with pronounced immunometabolic hyperactivation, which acts as a key driver of tubular injury in early DN. Through flow cytometry and functional analyses, we reveal that renal trNKs selectively expand in early DN and exhibit a unique hybrid hypermetabolic state characterized by the concurrent enhancement of glycolysis and oxidative phosphorylation. This bioenergetic adaptation orchestrated by pyruvate carboxylase (**Pcx**)-mediated tricarboxylic acid (TCA) cycle anaplerosis bypassing metabolic blockade and synergizing with myelocytomatosis oncogene **(Myc)**-driven transcriptional co-activation, fuels hyperactivated trNKs effector functions, notably driving inflammatory injury to neighboring tubular cells. Mechanistically, we attribute this hypermetabolic transition to upregulation of the aconitate decarboxylase 1 (ACOD1)-itaconate pathway, which paradoxically acts as a local metabolic amplifier rather than an anti-inflammatory brake in this context. Crucially, NK cell-specific deletion of *Acod1 (Ncr1-iCre Acod1*$^{fl/fl}$*)* or targeted metabolic intervention markedly attenuates early tubular damage. Collectively, our findings uncover a model of early renal trNKs accumulation and immunometabolic hyperactivation driving DN progression, highlighting local immunometabolic targeting as a promising therapeutic

strategy for early DN.

Keywords

Diabetic nephropathy; Tissue-resident natural killer cells; Itaconate; Immunometabolic reprogramming.

Introduction

Diabetic nephropathy (DN), a common microvascular complication of diabetes, is the leading cause of end-stage renal disease (ESRD) [1,2]. Although DN has long been considered a glomerulocentric disorder mediated by chronic hyperglycemia [3,4], the rapid progression of tubulointerstitial injury suggests a more complex and self-perpetuating inflammatory process that extends beyond the glomerulus [5-7]. Our previous work has directly linked immune cell activation to renal tubular injury in metabolic kidney disease [8,9]. Transcriptomic atlases, including datasets from our own models, show renal enrichment of pro-inflammatory immune subsets in DN [1,10]. Recent studies have expanded beyond systemic immunity to the local metabolic-immune circuits within kidneys [11], the primary site where resident cellular crosstalk drives progressive injury [12,13]. However, the metabolic cues that reprogram quiescent immune cells toward pathogenic effectors remain unclear. Effectively targeting these local circuits requires a granular understanding of how renal tissue-resident immune cells respond to the metabolic stress in the diabetic kidneys.

Natural killer (NK) cells are increasingly recognized as innate lymphocytes endowed with remarkable metabolic flexibility [14-16]. In diabetes, however, their function is frequently described as a systemically suppressed phenotype with reduced

cytotoxicity in the peripheral circulation [17,18]. This overlooks the distinct biology of tissue-resident NK cells (trNKs), which, unlike their circulating counterparts, permanently reside within renal tubulointerstitium [19,20]. Although recent studies have begun delineating the heterogeneity of kidney-resident immune cells [21], the function of trNKs during the onset of DN is still poorly understood. It remains unclear whether these cells act as merely bystanders in tubulointerstitium or as primary contributors to tubular interstitial inflammation, ultimately driving tubular atrophy and fibrosis [19].

Although itaconate is widely regarded as a universal metabolic brake on inflammation in macrophages, conferring cytoprotection through succinate dehydrogenase (SDH) inhibition [22,23] and multiple immunometabolic signalings pathways [24-28], emerging evidence suggests its function is exquisitely context- and cell-type-dependent [29-32]. Our previous work also demonstrated that bioenergetic metabolites could bypass their conventional metabolic roles and participate in pathological processes [33]. Whether non-myeloid, tissue-resident lymphocytes like renal trNKs co-opt or diverge from this classical paradigm under diabetic metabolic stress remains completely unknown.

In this study, we demonstrate that the expansion of renal trNKs exacerbates tubular injury in DN, through itaconate-mediated metabolic reprogramming and pro-inflammatory IFN-γ production. Mechanistically, trNKs exhibit concurrent OXPHOS and glycolysis enhancement by pyruvate carboxylase (Pcx)-mediated tricarboxylic acid (TCA) cycle anaplerosis and myelocytomatosis oncogene (Myc)-driven transcriptional

reprogramming. Critically, these findings challenge the conventional anti-inflammatory and cytoprotective role of itaconate in peripheral myeloid cells. NK cell-specific deletion of *Acod1* markedly attenuated renal tubular injury in DN. Thus, targeting local trNKs immunometabolism, specifically the ACOD1-itaconate axis, represents a promising non-immunosuppressive therapeutic strategy for DN.

Results

Expansion of renal trNKs in DN mice

Adaptation to the renal microenvironment endows trNKs with unique phenotypes and functions [19]. To comprehensively profile trNKs, we employed flow cytometry across various kidney diseases models. Notably, the proportion of renal trNKs was remarkably elevated in DN mice compared to models of sepsis-associated acute kidney injury (SA-AKI), obesity-related glomerulopathy (ORG), and lupus nephritis (LN) models (Fig. 1A, B and Supplementary Fig. 1A-C). Consistent with these findings, single-cell RNA sequencing (scRNA-seq) UMAP plots demonstrated a marked increase in the abundance (brown cluster) and spatial clustering of renal NK cells in DN (Fig. 1C).

Strikingly, compared with the normal control (NC) group, DN mice exhibited a marked expansion (approximately 35-fold) in the renal trNKs proportion (Fig. 1D). Conversely, the proportions of both B and T cells were significantly diminished in DN mice (Supplementary Fig. 1D). Cross-tissue comparison further revealed that this trNKs expansion was specifically enriched in the kidneys, compared with other systemic (blood, adipose), parenchymal (liver), or lymphoid (spleen) immune

compartments (Fig. 1D). Within renal tissues, NK cells differentiate into distinct subsets in response to microenvironmental cues [19]. In DN mice, renal trNKs (DN-trNKs) displayed a phenotype consistent with tissue retention, characterized by robust co-expression of CD69 (a C-type lectin receptor and early activation marker) [34] (Fig. 1E) and CD49a (α1 integrin) [35,36], alongside the absence of the circulating marker CD49b (Fig. 1F) [36]. Diabetic renal trNKs were therefore defined as a $CD3^{-}NK1.1^{+}CD69^{+}CD49a^{+}CD49b^{-}$ subset. Together, the progressive accumulation of trNKs and the concomitant reduction in adaptive lymphocytes (B/T cells) indicate a shift toward renal innate immunity in the pathogenesis of DN.

Adoptive transfer of DN-trNKs aggravates renal tubular injury

Given the marked expansion of DN-trNKs, an NK subset reported to predominantly localize to the tubulointerstitium [19,20], it's worth considering whether trNKs contribute to tubular injury in DN. As shown by IHC staining of human renal biopsy tissues, renal trNKs predominantly localize to the tubulointerstitium (Supplementary Fig. 1E). In clinical DN cohorts, we found that the abundance of renal trNKs positively correlated with the established tubular injury biomarkers (KIM-1 and NGAL), with the strongest associations observed in patients with early-stage DN (stages I-II) (Fig. 1G and Supplementary Fig. 1E, Tables S1-S6). To establish a causal relationship, we adoptively transferred trNKs from the NC group (NC-trNKs) and DN-trNKs into immunodeficient NOD-scid $IL2R\gamma^{-/-}$ (NSG) mice via intrarenal arterial injection (Fig. 1H). Effective engraftment of the transferred trNKs within the recipient kidneys was confirmed by flow cytometry (Supplementary Fig. 2A). Considering the role of NK

cells in mediating cytotoxicity upon activation [37], we further assessed the secretory profile of DN-trNKs. Enzyme-linked immunosorbent assay (ELISA) of renal tissues demonstrated enhanced secretion of inflammatory/cytotoxic mediators in DN-trNKs recipients, with the pro-inflammatory cytokine interferon-γ (IFN-γ) exhibiting the most significant elevation ($p < 0.001$) (Fig. 1I and Supplementary Fig. 2B). Additionally, the levels of cytotoxic granules (perforin and granzyme B), and tumor necrosis factor-α (TNF-α) were significantly upregulated in DN-trNKs group (Supplementary Fig. 2B). This enhanced inflammatory phenotype was further supported by flow cytometry, showing that the proportion of IFN-γ^+ trNKs was significantly increased in mice receiving DN-trNKs compared to those receiving NC-trNKs (Fig. 1J and Supplementary Fig. 2C)

Next, we evaluated the effects of DN-trNKs on renal function and tubular integrity. We found that adoptive transfer of DN-trNKs caused significant elevations in the renal dysfunction parameters, including serum creatinine (sCr), blood urea nitrogen (BUN), urinary microalbumin (Umalb), and urinary albumin-to-creatinine ratio (UACR) (Supplementary Fig. 2D). Furthermore, western blot (WB) analysis confirmed the upregulation of KIM-1 and NGAL in the renal tissues from DN-trNKs recipients (Fig. 1K). We proceeded to assess histological changes in the renal cortex of NSG mice. According to hematoxylin and eosin (H&E) (Fig. 1L) and periodic acid-Schiff (PAS) staining (Supplementary Fig. 2E), adoptive transfer of DN-trNKs induced substantial tubular injury, as determined by significantly elevated renal tubular injury scores. Consistent immunohistochemical (IHC) staining further confirmed overexpression of

KIM-1 and NGAL, predominantly localized to tubular lesions in DN-trNKs recipients (Fig. 1M). Therefore, these results elucidate a pathogenic role for trNKs in DN, demonstrating that these cells do not merely accumulate in the tubulointerstitium but actively promote tubular injury.

Depletion of NK cells ameliorates renal injury in DN

To further validate the pathogenic role of NK cells, we established a murine DN model by subjecting male C57BL/6J mice to a high-fat diet (HFD) and administering intraperitoneal streptozotocin (STZ) injections (Supplementary Fig. 3A, 3B). Prior to STZ administration, glucose tolerance test (GTT) (Supplementary Fig. 3D) and insulin tolerance test (ITT) (Supplementary Fig. 3E) analyses confirmed impaired glucose tolerance and reduced insulin sensitivity. Consistent with the development of hyperglycemia and glycosuria (Supplementary Fig. 3F, 3G), renal dysfunction parameters, including sCr, BUN, Umalb, and UACR were significantly elevated in DN mice (Supplementary Fig. 3J). Additionally, Masson's trichrome staining revealed no significant difference in collagen deposition (Supplementary Fig. 3C), confirming the establishment of an early-stage DN model prior to the onset of overt renal fibrosis. Furthermore, *in vivo* experiments revealed markedly elevated expression of KIM-1 and NGAL in renal tissues from DN mice (Supplementary Fig. 3H). *In vitro,* exposure of renal tubular epithelial cells (RTECs) to varying glucose concentrations revealed a dose-dependent upregulation of KIM-1 and NGAL, from normal glucose (NG, 5.5 mM) to moderate glucose (MG, 20 mM) and high glucose (HG, 40 mM) (Supplementary Fig. 3I). Comprehensive histopathological evaluations of renal cortex, including H&E, IHC,

and immunofluorescence (IF) staining, confirmed the presence of tubular injury in DN mice. Collectively, these results provide evidence that renal tubular injury occurs as a hallmark of early-stage DN.

Since adoptive transfer of DN-trNKs exacerbated tubular injury, we hypothesized that depleting NK cells would confer renoprotection. We administered the NK-depleting antibody PK136 [38] to evaluate its *in vivo* impact on renal tubular injury (Fig. 2A). Flow cytometry confirmed the efficacy of trNKs depletion (Fig. 2B). ELISA analysis showed significantly reduced renal level of IFN-γ (Fig. 2C), with minimal impact on perforin, granzyme B, or TNF-α (Supplementary Fig. 4A) following NK depletion. Consistent results of flow cytometry showed that the proportion of IFN-γ^+ trNKs was significantly decreased in NK-depleted DN mice (Fig. 2D).

Correspondingly, NK depletion effectively restored renal function, as evidenced by significantly decreased sCr, BUN, Umalb and UACR (Supplementary Fig. 4B). This functional recovery was accompanied by the downregulation of KIM-1 and NGAL, as confirmed by WB (Fig. 2E). Additionally, histological evaluation via H&E (Fig. 2F), PAS (Supplementary Fig. 4C) and IHC (Fig. 2G) staining further confirmed a marked alleviation of tubular injury scores and KIM-1/NGAL expression following NK depletion. Thus, these findings provide reciprocal evidence that NK cells contribute to tubular injury. This detrimental effect is primarily mediated by increased secretion of IFN-γ.

Concurrent enhancement of OXPHOS and glycolysis in DN-trNKs

To delineate the mechanisms underlying trNKs-induced tubular injury, we

investigated the metabolic reprogramming of these immune cells, a process reported to regulate inflammatory response [11,29]. We quantified the oxygen consumption rate (OCR) and extracellular acidification rate (ECAR) to evaluate mitochondrial respiration and glycolytic activity, respectively. Accordingly, compared to NC-trNKs, DN-trNKs exhibited substantially enhanced mitochondrial respiratory function (Fig. 3A), characterized by significant increases in basal respiration, ATP-linked respiration, maximal respiratory capacity (MRC), and spare respiratory capacity (SRC) (Fig. 3B). The elevated ATP-linked respiration highlights a reliance on oxidative phosphorylation (OXPHOS) for bioenergetic maintenance in DN-trNKs.

Regarding the glycolytic characteristics of DN-trNKs (Fig. 3C), DN-trNKs exhibited significantly enhanced glycolytic capacity when OXPHOS-derived ATP production was compromised by oligomycin, thereby enabling sustained biogenetic demands. Furthermore, basal glycolysis was comparable between the two groups, whereas glycolytic capacity and glycolytic reserve were significantly elevated in DN-trNKs (Fig. 3D), indicating a strong response to acute bioenergetic demands through glycolytic activation. Based on the immunometabolic reprogramming observed in DN-trNKs, we evaluated the proportion of ROS^+ trNKs between NC and DN mice by flow cytometry (Supplementary Fig. 3K). We found that ROS^+ trNKs did not differ significantly between NC and DN mice, suggesting that tubular injury is predominantly induced by inflammatory/cytotoxic effectors rather than direct oxidative stress. Thus, renal trNKs undergo immunometabolic reprogramming toward a hybrid hypermetabolic state, with concurrent enhancement of OXPHOS and glycolysis, to sustain the bioenergetic

demands of promoting tubular injury in DN.

IFN-γ from DN-trNKs mediates pro-inflammatory tubular injury

NK cells secrete an arsenal of inflammatory/cytotoxic mediators, with IFN-γ being a key mediator linked to renal injury [20,39-41]. As shown above, DN-trNKs in NSG mice exhibited markedly elevated secretion of the pro-inflammatory cytokine IFN-γ. We then established direct/Transwell trNKs-RTEC co-culture systems. Direct co-culture revealed that RTECs incubated with DN-trNKs exhibited elevated expression of KIM-1 and NGAL (Fig. 3E, F). Thus, this monolayer co-culture result validates the direct pathogenic role of DN-trNKs in tubular injury *in vitro*.

To elucidate whether trNKs-induced tubular injury is dependent on IFN-γ paracrine effects, we performed a Transwell assay and detected significantly elevated IFN-γ production from DN-trNKs in the RTEC supernatant (Fig. 3G, H), which could be neutralized by IFN-γ neutralizing monoclonal antibody (XMG1.2). Subsequent WB showed that RTECs seeded in the bottom chamber exhibited upregulation of KIM-1 and NGAL expression (Fig. 3I). Remarkably, this injury response was effectively attenuated by the introduction of XMG1.2. Consistently, *in vivo* assessment revealed significantly increased the renal IFN-γ level and IFN-γ^+ trNKs proportion in DN mice (Fig. 3J-L and Supplementary Fig. 4D-E), which paralleled exacerbated tubular injury, as assessed by WB (Fig.3M), and histopathological staining (Fig. 3N, O and Supplementary Fig. 4F). After XMG1.2 injection, a significant reduction was observed in the renal IFN-γ level (Fig. 3K), the proportion of IFN-γ^+ trNKs (Fig. 3L, Supplementary Fig. 4D, E) and renal tubular injury (Fig. 3M-O and Supplementary Fig.

4F). Thus, these findings demonstrate that pro-inflammatory IFN-γ released by DN-trNKs serves as a key pro-inflammatory mediator inducing renal tubular injury both *in vitro* and *in vivo*.

ACOD1 upregulation and OXPHOS enrichment in DN-trNKs

To further investigate the molecular mechanisms underlying the immunometabolic reprogramming of NK cells, we performed RNA-sequencing analysis (RNA-seq) on fluorescence-activated cell sorting (FACS)-sorted NC-trNKs and DN-trNKs (Fig. 4A). The volcano plot displayed the differentially expressed genes (DEGs) (Fig. 4B). The significant DEGs were then filtered, and the top15 up- and down-regulated DEGs were visualized in a heatmap (Fig. 4C). Notably, Acod1, an enzyme catalyzing itaconate production from TCA cycle intermediate *cis*-aconitate [22,24,42], emerged as the top-ranked upregulated DEG. We then performed a functional enrichment analysis of Gene Ontology (GO) (Fig. 4D) and Kyoto Encyclopedia of Genes and Genomes (KEGG) (Fig. 4E) to elucidate the functions of the DEGs. GO analysis highlighted enrichment in immune response and lymphocyte activation, and KEGG pathway analysis revealed significant enrichment of OXPHOS among DEGs in DN-trNKs.

We next validated the ACOD1 expression *in vitro* and *in vivo*. Acod1 mRNA levels exhibited an approximately 80-fold increase in transcript abundance in DN-trNKs, with concordant validation by reverse transcription quantitative polymerase chain reaction (RT-qPCR) (Fig. 5I). Consistent with this, WB showed that ACOD1 protein levels were elevated in DN-trNKs (Fig. 4F), and glucose exposure elevated ACOD1 expression in a concentration-dependent manner (Fig. 4G). Furthermore, to visualize the expression

and localization of ACOD1, we performed IF co-staining (CD3/NK1.1/ACOD1) (Fig. 4H), alongside IHC staining on mouse and human kidney sections (Supplementary Fig. 5A-D). Consistent with the tubulointerstitial localization of trNKs [19,20], ACOD1 expression was distinctly upregulated in trNKs in the DN group, with pronounced staining localized to renal tubulointerstitium, but undetectable expression in the glomeruli. Collectively, this spatial and quantitative profile suggests that ACOD1 upregulation in DN-trNKs is closely associated with the pathogenesis of tubular injury in DN.

Itaconate confers no renoprotection, but even causes damage to tubules in DN

ACOD1 is known for catalyzing *cis*-aconitic acid to generate the immunoregulatory metabolite itaconate. Itaconate is esterified to cell-permeable derivatives (dimethyl- and 4-octyl-itaconate) (Fig. 5A) [43]. Consistent with ACOD1 upregulation, ELISA analysis revealed that itaconate levels were significantly increased in DN-trNKs (Fig. 5B). Based on previous evidence that itaconate confers cytoprotection and reduces ROS production via TCA cycle blockade [22,23], we next investigated whether its exogenous administration could attenuate tubular injury in DN (Fig. 5C). We first assessed the effect of itaconate on respiratory function in trNKs. Unexpectedly, OCR measurements revealed that itaconate treatment enhanced OXPHOS of DN-trNKs (Fig. 5D), as evidenced by increased basal and ATP-linked respiration, MRC, and SRC (Supplementary Fig. 6A). We proceeded to evaluate its *in vivo* effect on tubular injury. Contrary to its conventional cytoprotective effect, treatment with itaconate or its cell-permeable derivative 4-octyl-itaconate (4-OI) failed to improve renal function in DN

mice, as sCr, BUN, Umalb, and UACR remained persistently elevated (Supplementary Fig. 6B). As for tubular injury, WB (Fig. 5E) indicated elevated protein levels of KIM-1 and NGAL. Moreover, histopathological evaluation via H&E and PAS staining demonstrated aggravated tubular injury scores (Fig. 5F and Supplementary Fig. 6D), and IHC staining showed enhanced tubular KIM-1 and NGAL expression, following itaconate and 4-OI treatment (Fig. 5G).

In contrast, inhibition of itaconate production with IRG-IN1 markedly attenuated these pathological changes. Specifically, IRG-IN1 treatment significantly reduced the elevated levels of sCr, BUN, Umalb and UACR (Supplementary Fig. 6B). Furthermore, IRG-IN1 administration effectively downregulated the expression of KIM-1 and NGAL (Fig. 5E, G), and decreased the tubular injury scores (Fig. 5F and Supplementary Fig. 6D). Therefore, these findings fundamentally challenge the prevailing assumption that itaconate is a broadly protective immunometabolite, demonstrating instead that it offers no renoprotection against tubular injury in DN and may even exacerbate pathology.

NK cell-specific Acod1 knockout ameliorates tubular injury in DN

To definitively determine establish the cell-type-specific role of ACOD1 *in vivo*, we crossed *Acod1*^{floxflox} (*Acod1*$^{fl/fl}$) mice with *Ncr1*-iCre mice to generate mice with Acod1 knockout restricted to NK cells (*Ncr1-iCre Acod1*$^{fl/fl}$) (Fig. 5H). Both genotypes underwent DN induction with HFD/STZ, with a subset of *Ncr1-iCre Acod1*$^{fl/fl}$ mice receiving 4-OI treatment. Successful knockout of Acod1 was confirmed by genotyping analysis (Supplementary Fig. 5E), and further validated by RT-qPCR in sorted trNKs (Fig. 5I). Next, we performed IF co-staining (ACOD1/KIM-1), showing that ACOD1

311 expression was efficiently depleted in the trNKs in *Ncr1-iCre Acod1*$^{fl/fl}$ mice (Fig. 5M).

312 Since itaconate has no protective effect in DN, we next investigated whether Acod1
313 knockout alleviates tubular injury in DN. Consistent with this hypothesis, NK-specific
314 Acod1 knockout improved renal function in DN, with decreased levels of sCr, BUN,
315 Umalb and UACR (Supplementary Fig. 6F). Furthermore, histological evaluation was
316 conducted on the renal cortex. Compared with WT (NC) mice, H&E (Fig. 5J) and PAS
317 (Supplementary Fig. 6G) staining demonstrated a significant increase in the tubular
318 injury scores in WT + HFD/STZ (DN) mice. Transmission electron microscopy (TEM)
319 revealed severe tubular ultrastructural disruption in HFD/STZ mice, including focal
320 loss of brush-border microvilli and mitochondrial swelling with disorganized cristae
321 (Fig. 5K). IHC analysis of the renal cortex revealed a substantial increase in KIM-1 and
322 NGAL expression in HFD/STZ mice (Fig. 5L).

323 Importantly, NK cell-specific Acod1 knockout significantly improved renal function
324 in HFD/STZ mice (Supplementary Fig. 6F). H&E and PAS staining further revealed
325 improved tubular injury scores (Fig. 5J and Supplementary Fig. 6G), along with an
326 alleviation of tubular ultrastructural disruption based on TEM (Fig. 5K) in *Ncr1-iCre*
327 *Acod1*$^{fl/fl}$ + HFD/STZ mice, as compared with WT + HFD/STZ and *Acod1*$^{fl/fl}$ +
328 HFD/STZ mice. Consistently, IHC staining showed decreased KIM-1 and NGAL
329 staining in *Ncr1-iCre Acod1*$^{fl/fl}$ + HFD/STZ mice compared with WT + HFD/STZ and
330 *Acod1*$^{fl/fl}$ + HFD/STZ mice (Fig. 5L).

331 To simultaneously evaluate the ACOD1 expression and renal tubular injury, we
332 performed the IF co-staining of ACOD1 and KIM-1 (Fig. 5M). The expression of

ACOD1 and KIM-1 was markedly elevated in WT + HFD/STZ mice compared to WT mice, as quantified by ACOD1 and KIM-1 positive tubules. Crucially, this upregulation was markedly reversed in *Ncr1-iCre Acod1*$^{fl/fl}$ + HFD/STZ mice, compared with WT + HFD/STZ and *Acod1*$^{fl/fl}$ + HFD/STZ mice. However, exogenous supplementation with 4-OI to *Ncr1-iCre Acod1*$^{fl/fl}$ + HFD/STZ mice abrogated the renoprotective effect and even exacerbated tubular injury, further supporting the pathogenic role of itaconate (Fig. 5J-M and Supplementary Fig. 6F, G). Collectively, ACOD1 upregulation in NK cells mediates tubular injury in DN, with itaconate serving as the key functional metabolite.

Pcx-mediated TCA anaplerosis and Myc-driven transcriptional reprogramming counteract itaconate induced TCA truncation in DN-trNKs

Of particular interest, although itaconate is known to blockade the TCA cycle via SDH suppression, our metabolic profiling unexpectedly revealed a concurrent enhancement of OXPHOS and glycolysis in DN-trNKs (Fig. 3A-3D). This paradoxical metabolic reprogramming prompted us to investigate how DN-trNKs maintain TCA cycle flux and achieve a hybrid hypermetabolic phenotype despite itaconate-induced metabolic blockade.

Metabolic enrichment analysis identified coordinated activation of OXPHOS, glycolysis and TCA cycle in DN-trNKs, with pyruvate metabolism emerging as a pivotal pathway (Fig. 6A). To identify key regulators bridging TCA and pyruvate metabolism, we intersected upregulated DEGs in both pathways. Accordingly, nine overlapping genes were identified, among which Pcx was the top-ranked candidate (Fig. 6B). Its protein product PCX was markedly upregulated in DN-trNKs, as confirmed by

WB (Fig. 6C). Consistently, compared with WT mice, WB analysis revealed a marked upregulation of PCX protein level in the renal tissues of WT + HFD/STZ mice. Importantly, NK cell-specific Acod1 knockout significantly reduced PCX expression in HFD/STZ mice. However, exogenous administration of 4-OI to Ncr1-iCre Acod1$^{fl/fl}$ + HFD/STZ mice significantly restored PCX expression (Fig. 6D). This result suggested an important role for pyruvate-dependent anaplerosis in TCA restoration. Additionally, Sankey diagram identified Myc as the key overlapping regulator across OXPHOS, glycolysis, and pyruvate metabolism (Fig. 6E), with elevated MYC protein level verified by WB (Fig. 6F). Myc has been recognized as a transcription factor that enhances both OXPHOS and glycolysis to sustain bioenergetic demands [44,45], elegantly explaining the hybrid hypermetabolic phenotype of DN-trNKs.

As schematized in Figure 6G, RNA-seq and RT-qPCR results validated the upregulation of mRNA levels of Acod1, Pcx and Myc, but the downregulation of pyruvate dehydrogenase E1 alpha 1 subunit (Pdhα1) and succinate dehydrogenase complex subunit A (Sdhα) in DN-trNKs. At the protein level, ACOD1-catalyzed itaconate production blocks TCA via SDH inhibition, while PDH downregulation redirects pyruvate toward PCX-mediated anaplerosis to replenish TCA intermediates. Concurrently, MYC co-activates both OXPHOS and glycolysis. Together, these two mechanisms account for the hybrid hypermetabolic phenotype in DN-trNKs.

Itaconate promotes IFN-γ production from DN-trNKs, whereas NK cell-specific Acod1 knockout suppresses this pro-inflammatory response

Although itaconate is conventionally recognized as an anti-inflammatory metabolite

in macrophages, emerging evidence suggests that metabolic reprogramming can sustain the bioenergetic demands of the pro-inflammatory functions of immune cells [11,29]. Based on our data showing that ACOD1-upregulated DN-trNKs contributed to tubular injury through IFN-γ production, we proceeded to examine the role of ACOD1 in this pro-inflammatory response. As displayed in a Sankey diagram, GO analysis of inflammation related pathways in DN-trNKs revealed that DEGs were significantly enriched in IFN-γ production (Fig. 7A). This was further supported by Gene set enrichment analysis (GSEA) (Fig. 7B), suggesting that DN-trNKs were positively associated with innate immune response (GO:0045087), IFN-γ production (GO:0032609), NK cell activation (GO:0050854) and NK cell-mediated immunity (GO:0002228). In addition, a broad range of genes related to IFN-γ production was upregulated in DN-trNKs, including cytokines (e.g., IL-12a, IL-12b and IL-18), surface receptors (e.g., *Klrk1*, *Cd226* and *Slamf6*) and transcription factors (e.g., *Runx3* and *Irf8*) (Fig. 7C, D).

Given the reported role of itaconate in inhibiting type I IFN signaling [46], we next examined whether itaconate could suppress this pro-inflammatory response. Contrary to this expectation, ELISA revealed that itaconate/4-OI treatment unexpectedly paradoxically failed to reduce the IFN-γ production in DN mice (Fig. 7E). Indeed, we observed an increased trend in IFN-γ level. The levels of granzyme B, perforin, and TNF-α remained unchanged (Supplementary Fig. 6C). We next performed flow cytometry to quantify the proportions of trNKs and their IFN-γ production. In DN mice, itaconate/4-OI treatment failed to reduce the proportions of trNKs and IFN-γ^+ trNKs, instead showing an upward trend (Fig. 7F, G). In contrast, pharmacological inhibition

of ACOD1 by IRG-IN1 significantly suppressed the renal IFN-γ level, and the proportions of trNKs and IFN-γ^+ trNKs in DN.

Finally, we profiled the inflammatory response of trNKs from the conditional knockout mice. ELISA revealed that NK-specific Acod1 knockout induced a significant downregulation of renal IFN-γ (Fig. 7H), alongside perforin, granzyme B, with the exception of TNF-α (Supplementary Fig. 6E). Flow cytometry further confirmed a significant reduction in the proportions of trNKs (Fig. 7I) and IFN-γ^+ trNKs (Fig. 7J) in *Ncr1-iCre Acod1*$^{fl/fl}$ + HFD/STZ mice, as compared with WT + HFD/STZ and *Acod1*$^{fl/fl}$ + HFD/STZ mice. Crucially, administration of 4-OI to the conditional knockout mice reversed this amelioration, effectively restoring the renal IFN-γ production, and the proportions of trNKs and IFN-γ^+ trNKs (Fig. 7H, J). Taken together, these data establish that the ACOD1-itaconate axis contributes to the renal residency and pro-inflammatory function of DN-trNKs. Targeted deletion of Acod1 alleviates tubular injury in DN by abrogating itaconate-driven IFN-γ overproduction from DN-trNKs, thereby uncoupling the immunometabolic circuit that drives DN progression.

Discussion

The principal finding of this study is that the expansion of renal trNKs exacerbates tubular injury in DN, through itaconate-mediated metabolic reprogramming, and a paradoxical pro-inflammatory response. This result directly challenges the conventional role of itaconate as an anti-inflammatory and cytoprotective metabolite [22,24-27], and extends the immunomodulatory role of the ACOD1-itaconate axis beyond the myeloid lineage into the lymphoid compartment. Notably, DN-trNKs display a distinct hybrid hypermetabolic phenotype characterized by concurrent

enhancement of OXPHOS and glycolysis. To sustain these profound bioenergetic demands and counteract itaconate-induced TCA truncation, we propose a coordinated mechanism whereby Pcx-mediated TCA anaplerosis functions with Myc-driven transcriptional reprogramming. Despite growing advocacy for itaconate-based clinical interventions in inflammatory diseases [47-49], our work critically demonstrates that the immunomodulatory effects of itaconate are highly context-dependent, dictated by the tissue microenvironment and resident cell type.

It is important to distinguish our findings from previous studies on itaconate in circulating myeloid cells or systemic immunity. While itaconate suppresses macrophage activation in acute systemic inflammation, renal trNKs operate within a chronically hyperosmotic and lipid-rich tubulointerstitial microenvironment. In this distinct niche, itaconate production does not extinguish inflammation; instead, it acts as a metabolic trigger for sustained IFN-γ release. Furthermore, we solve the metabolic dilemma of how cells survive itaconate-mediated SDH suppression by uncovering the Pcx-anaplerosis bypass and Myc co-activation. This conceptual advance redefines the boundary of itaconate biology from a purely immunosuppressive metabolite to a tissue-specific immunometabolic tuner.

Extending our prior work linking immune cells to renal tubular injury in metabolic kidney disease [8,9], we now delineate a pathogenic role for renal trNKs in early DN through local immunometabolic reprogramming. Consistent with trNKs previously identified in non-lymphoid tissues, including the liver [50], lungs [36], and colon [51], renal trNKs also represent a subset endowed with tissue-adapted characteristics [19].

Even under identical systemic conditions, DN-trNKs remain phenotypically and functionally distinct from both circulating NK (cNK) cells and NK cells residing in non-renal tissues [19,52]. In our study, by employing systemic perfusion to rigorously exclude cNK cells, we confirmed a marked expansion of renal trNKs expressing residency markers CD69 [34] and CD49a [35,36]. Anatomically resident within the renal tubulointerstitium, these trNKs facilitate local cellular crosstalk, thereby rendering adjacent tubular epithelium highly susceptible to injury [19,20]. Although DN is classically considered a glomerulocentric disease [3,4], tubulointerstitial trNKs acquire a kidney-specific phenotype that enables their direct contribution to tubular injury. Our finding that previously unappreciated lymphocyte subsets expand in diabetic kidneys suggests their pathogenic involvement in DN. Functionally, adoptive transfer of DN-trNKs into non-diabetic recipients was sufficient to exacerbate renal tubular injury, even in the absence of hyperglycemia or other diabetic stimuli. In contrast, adoptive transfer of NC-trNKs failed to elicit comparable tubular injury. Collectively, these results provide definitive and causal evidence that renal trNKs are not merely tubulointerstitial bystanders, but primary contributors to tubular injury in DN.

Having established the pathogenic role of DN-trNKs, we next sought to investigate whether immunometabolic reprogramming accounts for the pathogenic function of DN-trNKs. A striking observation in our study is that DN-trNKs displayed the concurrent elevation of OXPHOS and glycolysis within the diabetic kidneys. This hybrid metabolic phenotype diverges from the classical Warburg effect, traditionally

attributed to irreversible mitochondrial damage and aerobic glycolytic reliance [53,54]. Instead, trNKs exhibit metabolic flexibility, engaging a distinct hybrid hypermetabolic program to support the high bioenergetic and biosynthetic demands of persistent inflammatory cytokine production. Accumulating evidence indicates that NK cells exacerbate renal tubular injury and interstitial fibrosis by secreting inflammatory/cytotoxic mediators, particularly IFN-γ [20,41,55]. Consistently, renal trNKs display an augmented pro-inflammatory response in DN. In adoptive transfer experiments, several cytotoxic and pro-inflammatory mediators were elevated. Among them, IFN-γ exhibited the strongest correlation with tubular injury, and showed the most pronounced increase (approximately 3-fold). Subsequent direct/Transwell coculture experiments further confirmed that IFN-γ production endows trNKs with capacity to initiate and propagate tubular injury. Therefore, trNKs emerge not as tubulointerstitial bystanders in the diabetic kidneys, but as tissue-specific effectors that convert local inflammatory signals into tubular injury in DN.

Building on the functional characterization of trNKs, we then identified the ACOD1-itaconate axis as a key mediator of their pathogenic transformation in DN. Itaconate in activated myeloid cells is conventionally regarded as anti-inflammatory, exerting its effects primally through SDH inhibition [22], NRF2 activation [24] and NLRP3 inflammasome inhibition [25]. However, our findings revealed a striking kidney-resident exception, which parallels the recently described pro-inflammatory effect in alveolar-resident macrophages [29]. In our study, ACOD1 is a critical determinant of trNKs induced tubular injury. The marked upregulation of ACOD1 in

DN-trNKs (approximately 80-fold) suggests a kidney-specific metabolic adaptation that redirects citrate flux toward itaconate production [47,56]. However, aberrant TCA flux and intermediate accumulation, as exemplified by ACO2 regulation, directly cause renal tubular dysfunction [56]. Moreover, our experiments demonstrated that ACOD1 is preferentially expressed in the tubulointerstitium rather than the glomeruli, aligning with the renal distribution of trNKs. This spatial congruence supports our focus on tubular injury, rather than glomerular pathology, as the renal outcome of trNKs-mediated inflammation in DN. Furthermore, we have previously demonstrated that bioenergetic metabolites can act beyond their conventional metabolic functions and directly contribute to disease pathogenesis [33]. In this study, contrary to the expected anti-inflammatory benefits, exogenous itaconate/4-OI treatment fails to suppress IFN-γ production and even exacerbates tubular injury in DN. Indeed, we observed an increasing trend in trNKs proportion and IFN-γ level following treatment, thereby reinforcing the pathogenic role of itaconate in DN. Conversely, NK-specific Acod1 knockout *in vivo* (*Ncr1-iCre Acod1*$^{fl/fl}$ mice) significantly decreased IFN-γ production, attenuated tubular injury and preserved renal function in DN. By establishing the ACOD1-itaconate axis of trNKs as a previously unrecognized contributor to DN, our work offers a strategy for selectively halting DN progression by targeting this local immunometabolic circuit, without compromising systemic innate immune surveillance.

Of particular interest is why DN-trNKs displayed the concurrent enhancement of OXPHOS and glycolysis despite itaconate-induced TCA truncation. By competing with succinate, itaconate inhibits the TCA cycle enzyme SDH, thereby blocking succinate

511 oxidation and dampening OXPHOS [22,23]. In our previous studies, we found that cells
512 encountering metabolic stress engage metabolic flexibility, including 6PGDH-
513 mediated flux rearrangement [57,58] and LDHA-mediated energetic regeneration [33],
514 in OXPHOS or glycolysis to sustain bioenergetic demands. In this study, Pcx-mediated
515 anaplerosis has been demonstrated to replenish TCA cycle intermediates in
516 metabolically active immune cells, such as cytotoxic $CD8^+$ T cells[59]. Itaconate
517 production is closely linked to TCA anaplerosis, as its synthesis from *cis*-aconitate
518 relies on anaplerotic carbon flux [60]. In our study, RNA-seq with experimental
519 validation showed marked Pcx upregulation in DN-trNKs, with enrichment of the
520 pyruvate metabolic pathway. PDH suppression redirects pyruvate away from acetyl-
521 CoA generation toward Pcx-mediated anaplerosis, which replenishes oxaloacetate and
522 sustains intermediates of TCA flux [61,62]. We therefore propose that the elevated
523 OXPHOS in DN-trNKs is sustained through Pcx-mediated anaplerosis and
524 maintenance of TCA cycle flux. In addition, our previous work has demonstrated that
525 transcriptional reprogramming directly enhances OXPHOS and ATP production to
526 promote pathological proliferation [63]. Another interesting finding is that Myc, a
527 transcription factor that co-activates OXPHOS and glycolysis, was also markedly
528 upregulated in DN-trNKs. Myc has been shown to regulate NK cell development [64],
529 regulating NK cell metabolism by transcriptionally coordinating OXPHOS and
530 glycolysis [65,66]. Myc is also indispensable for IL-2/IL-12-induced glycolysis and
531 OXPHOS in NK cells, and Myc-deficient NK cells exhibit reduced IFN-γ and
532 granzyme B production [66]. Therefore, Pcx-mediated TCA anaplerosis and Myc-

driven transcriptional reprogramming synergistically sustain the bioenergetic demands of activated immune cells, elegantly explaining the hybrid hypermetabolic phenotype of DN-trNKs.

In conclusion, the ACOD1 in trNKs, contrary to its conventional anti-inflammatory and cytoprotective role, contributes to tubular injury in DN through a hybrid hypermetabolic state sustained by Pcx and Myc. Our work critically reveals that the immunomodulatory functions of itaconate are highly tissue- and cell-type-dependent. Targeting the ACOD1 within renal trNKs immunometabolism thus represents a promising non-immunosuppressive therapeutic strategy for DN.

Materials and methods

Patients and biopsy renal samples

Renal biopsy specimens were obtained from 39 DN patients [67,68], and were classified by the Renal Pathology Society (RPS) criteria [69]. This study complied with the Declaration of Helsinki. Written informed consent was obtained from all renal tissue donors. All procedures were approved by Human Ethics Committee of the First Affiliated Hospital of Jinan University (No. KY-2025-095). Detailed clinical information is provided in Tables S7 and S8 and the Supplemental Methods.

Animal Studies

All procedures involving experimental animals were performed following protocols approved by the Committee for Animal Research of Jinan University (No. IACUC-20250107-03) and conformed to the Guide for the Care and Use of Laboratory Animals.

Generation of NK-specific Acod1-knockout mice and genotyping

555 *Acod1*$^{fl/fl}$ and Ncr1-iCre mice on a C57BL/6J background were purchased from
556 Cyagen Biosciences Inc (Guangzhou, China). Ncr1-iCre; *Acod1*$^{fl/fl}$ mice were generated
557 by crossing *Acod1*$^{fl/fl}$ mice with Ncr1-iCre mice. Littermate *Acod1*$^{fl/fl}$ mice without Cre
558 served as controls. Genotyping was performed by PCR using tail genomic DNA (Primer
559 sequences are listed in Table S9). Knockout efficiency was verified by RT-qPCR in
560 FACS-sorted trNKs. Detailed animal procedures are provided in the Supplemental
561 Methods.

562 **Immunodeficient mice and adoptive transfer of trNKs**

563 Male NSG mice (8 weeks old) were purchased from Guangzhou Bojin
564 Biotechnology Co., Ltd. NSG recipients underwent adoptive transfer of vehicle, NC-
565 trNKs, and DN-trNKs (6×10^5 trNKs dissolved in 100μL sterile PBS). Renal tissue-
566 localizing trNKs accumulation was achieved by intrarenal artery injection, as
567 previously described [70,71]. 24-hour urine samples were collected using metabolic
568 cages. The engraftment of transferred trNKs in the recipient kidneys was confirmed by
569 flow cytometry at 24 hours post-transfer. Detailed surgical procedures for intrarenal
570 arterial injection are provided in the Supplemental Methods.

571 **High-fat diet / streptozotocin-induced DN in Mice**

572 To induce DN, mice were fed a HFD combined with intraperitoneal STZ injection,
573 as described by other studies (see Supplemental Methods for details) [72,73]. The
574 homozygous *Acod1*$^{fl/fl}$ mice and *Ncr1-iCre Acod1*$^{fl/fl}$ transgenic mice were further
575 subjected to DN induction by HFD/STZ administration, with a subset receiving 4-OI
576 treatment. Diabetic tubular injury was assessed by integrating histological evaluation

of tubular pathology with measurement of renal tubular injury markers.

***In vivo* monoclonal antibody treatment**

A separate cohort of mice was intravenously injected with monoclonal antibodies via inner canthus veniplex from the day of STZ injection until the end of the experiment. For NK cell depletion, mice received isotype-matched mouse IgG2a (IgG control; MedChemExpress) or anti-NK1.1 mAb (PK136; 200 μg/mouse, every 5 days; BioLegend) [74,75]. The efficiency of NK cell depletion was confirmed by flow cytometry, consistently exceeding 90%. For IFN-γ neutralization, mice were treated with anti-mouse IFN-γ neutralizing antibody (XMG1.2, 200μg/mouse, every 3 days; MACKLIN) [76]. The efficiency of IFN-γ blockade was confirmed by ELISA and flow cytometric analysis. For itaconate administration, mice received itaconate/4-OI (50 mg/kg and 25mg/kg, respectively; every 2 days; MACKLIN) [77,78] and the ACOD1 inhibitor (IRG1-IN-1, 0.5 mg/kg, every 2 days; MedChemExpress) [79,80].

Biochemical measurements

Biochemical parameters of serum samples (sCr, BUN, FBG) and urinary samples (urinary creatinine and umalb) were measured with commercial kits according to the manufacturers' protocols. Measurements were performed in triplicate at optimized wavelengths (500-640 nm) using a reaction temperature control system (37 °C). The urine albumin was normalized to urine creatinine.

RTEC culture and treatment

Transformed C3H mouse kidney-1 (TCMK-1) cells were purchased from the Warner Biotechnology Co., Ltd. (Wuhan, China). TCMK-1 cells were cultured in minimum

essential medium (MEM) (L550KJ, BasalMedia) containing 10% fetal bovine serum (Gibco, USA) and 1% penicillin–streptomycin (Gibco) at 37 °C in 5% CO_2. The medium was changed daily. TCMK-1 cells were exposed to complete medium containing 20 mM or 40 mM D-glucose (HG) for 48 h. The control groups received 5.5 mM D-glucose (NG) or mannitol (osmotic control).

trNKs co-culture experiments

Renal trNKs and RTECs were co-cultured in direct contact or in 24-well Transwell plates at a 1:10 ratio. For direct co-culture, trNKs were co-cultured with RTECs in 6-well plates for 24 hours. For Transwell co-culture, trNKs were seeded in the upper chambers, while RTECs were seeded into the bottom chamber for 24 hours [81,82]. Following co-culture, IFN-γ concentrations in the supernatants were determined by ELISA. RTECs were harvested with trypsin for subsequent experiments.

Renal tissue dissociation and single-cell suspension preparation

To remove erythrocytes and circulating leukocytes, euthanized mice were subjected to intracardiac perfusion with PBS via the right ventricle. Kidneys were minced into 1 mm^3 fragments and digested in 10 mL of digestion solution containing 1 mg/mL Collagenase Type IV (Worthington Biochemical) and 20 μg/mL DNase I (MilliporeSigma), at 37 °C for 30 min with agitation at 200 rpm. Cell suspension was filtered through 70 μm strainers, and residual erythrocytes were lysed on ice using red blood cell lysis solution (BioLegend). Cells were resuspended in 35% Percoll solution (Cytiva) and subjected to density-gradient centrifugation. The resulting single-cell suspensions were filtered through 70 μm strainers for subsequent experiments.

FACS sorting and primary culture of trNKs

To isolate renal trNKs, the single cell suspensions were stained with specific surface markers for 30 minutes (see flow cytometry panels in Supplemental Methods), washed twice and resuspended in FACS buffer (2% FBS in 1×PBS). Live/dead cell discrimination was performed by co-staining with 7-aminoactinomycin D (7-AAD; Invitrogen). Renal trNKs were isolated by FACS on the BD FACS-ARIA II cell sorter (BD Biosciences, USA). The sorted renal trNKs were cultured in RPMI 1640 medium supplemented with 10% FBS and 1% penicillin-streptomycin in 96-well plates, or directly used for subsequent experiments [83].

Flow cytometry analysis

Single-cell suspensions were prepared from the kidneys, liver, spleen, adipose tissue and peripheral blood. Cells were subsequently stained with the fixable viability dye BV510 (Invitrogen). Fc receptors were blocked using anti-CD16/32 (Tonbo Bioscience) at 4 °C for 15 minutes. For surface markers analysis, cells were stained in PBS with fluorophore-conjugated antibodies at pre-determined concentrations at 4 °C for 30 min. trNKs were identified as $CD69^{+}CD49a^{+}CD49b^{-}$ within the $NK1.1^{+}$ gate. For intracellular cytokine staining, cells were stimulated for 4-6 hours with Brefeldin A (BFA; Invitrogen; 1 μg/mL) at 37°C in a 5% CO_2 incubator, followed by fixation and permeabilization using Fixation/Permeabilization solution at 4 °C for 20 minutes. Intracellular staining was then performed with antibody against IFN-γ. Cells were then washed with 1× BD Perm/Wash™ buffer and resuspended in PBS for flow cytometry analysis on the BD FACSCanto flow cytometry system (BD Biosciences, USA). Data

were analyzed with FlowJo v10.8.0 Software. Flow cytometry panels are provided in Supplemental Methods.

Western blot

Protein lysates from trNKs, RTECs, and kidney tissues were analyzed by WB following established protocols. Protein expression was detected with primary antibodies against KIM-1, NGAL, ACOD1, PCX and MYC, with GAPDH or β-actin as loading control. Immunoreactive bands were visualized following incubation with horseradish peroxidase (HRP)-conjugated secondary antibodies. Detailed protocols and antibody information are provided in the Supplemental Methods.

Real-time quantitative polymerase chain reaction analysis

Total RNA was extracted from trNKs, RTECs, and kidney tissues using TRNzol Reagent (Tiangen Biotech, Beijing). The FastSensi gDNA dispelling RT SuperMix kit (Tiangen Biotech) was used to recerse the extracted RNAs into cDNA. The mRNA levels of Acod1, Pcx, Myc, Pdhα1 and Sdhα were determined by SYBR Green PCR Master Mix (Applied Biosystems, USA) using BioRad CFX-96 real-time system (BioRad, USA) (Primer sequences are listed in Table S10). The mRNA levels were normalized to GAPDH. Relative expression levels were quantified using $2^{-\Delta\Delta CT}$method.

Renal histology

Kidney sections were stained with H&E, PAS, and Masson's trichrome. Tubular injury was scored semiquantitatively (0-4) [84,85]. All histological evaluations were performed blinded to group allocation. Detailed staining procedures were provided in the Supplemental Methods.

Immunohistochemistry and immunofluorescence

For IHC, paraffin-embedded kidney sections were deparaffinized, rehydrated, and subjected to antigen retrieval. Sections were incubated overnight at 4°C with primary antibodies against KIM-1, NGAL, and ACOD1. For IF co-staining, kidney sections were incubated with primary antibodies against KIM-1, ACOD1, CD3 and NK1.1, followed by fluorophore-conjugated secondary antibodies (Alexa Fluor 488, 594, or 450; Invitrogen). Nuclei were counterstained with DAPI. Detailed protocols and antibody information are provided in the Supplemental Methods.

Transmission electron microscopy

The length of tubular microvillus, mitochondrial percentage, and mitochondrial length/width ratio in renal tubules were quantified from TEM images using ImageJ software. Detailed TEM procedures are provided in the Supplemental Methods.

Enzyme-linked immunosorbent assay

The levels of IFN-γ in cell supernatants and renal tissues, as well as TNF-α, perforin, granzyme B in renal tissues were measured using mouse ELISA kits (MEIMIAN, Jiangsu Meimian Industrial Co., Ltd.) according to the manufacturer's instructions. Absorbance (optical density, OD) was obtained at 450 nm using a microplate reader (Infinite F50, Tecan). Concentrations of NK inflammatory/cytotoxic mediators were determined by comparing the OD values against a standard curve. The intra-assay coefficient variation and the inter-assay variation are listed in Table S11.

Oxygen consumption rate analysis

Mitochondrial respiratory of sorted trNKs (1×10^6 cells/mL) was analyzed using

Oxygraph-2k respirometer. Following baseline stabilization, sequential titration was performed with oligomycin, carbonyl cyanide m-chlorophenyl hydrazone, rotenone, antimycin A. Data were acquired and analyzed using DatLab 7.4. Detailed procedures are provided in the Supplemental Methods.

Extracellular acidification rate analysis

Glycolytic function of trNKs (5×10^4 cells/well) was measured using a Seahorse XFe96 Analyzer. The glycolytic stress test was performed by sequential injections of glucose, oligomycin, and 2-DG. Data were normalized to live cell counts. Detailed procedures are provided in the Supplemental Methods.

RNA-sequencing analysis of trNKs

Renal trNKs (a $NK1.1^+CD69^+CD49^+CD49b^-$ subset) were FACS-sorted from NC and DN mice. Transcriptome profiling was performed on an Illumina Novaseq 6000 platform. DEGs were identified via DESeq2/edgeR, followed by GO and KEGG enrichment analysis. GSEA was performed to identify significantly enriched pathways. Detailed analytical procedures are in the Supplemental Methods.

scRNA-seq data processing and analysis

scRNA-seq data (GSE261356) from NC and DN mice were downloaded from Gene Expression Omnibus (GEO) database and analyzed using Seurat R package. Following quality control, data were normalized and batch-corrected using Harmony. Cell clusters were identified by Principal component analysis (PCA) and graph-based unsupervised clustering. Detailed bioinformatics pipelines are in the Supplemental Methods.

Cell type annotation

Cell clusters were annotated by integrating SingleR and the CellMarker database with reported marker genes. NK cells were validated by the expression of *Nkg7*, *Cd3g*, and *Cd3e*. Detailed procedures are in the Supplemental Methods.

Statistical analysis

Data are presented as mean ± standard deviation, from at least three independent experiments. Two-tailed unpaired Student's t test compared two groups, while one-way or two-way analysis of variance (ANOVA) followed by Tukey's post hoc test was employed for multiple comparisons. Statistical analyses were conducted using R (version 4.3.2) or GraphPad Prism 10.0 software. Differences with $P < 0.05$ were considered statistically significant.

Data and code availability

Public Gene Expression Omnibus (GEO) database (scRNA-seq dataset GSE261356) was referenced in this study. The raw reads of our transcriptome data have been deposited into the NCBI Short Read Archive (SRA, http://www.ncbi.nlm.nih.gov/sra/) under accession number PRJNA1516674. Additional information required to reanalyze the data is available from the lead contact upon request.

References

1. A cell atlas charts the immune architecture of diabetic kidney disease. Nature. 2026.
2. Himmelfarb J, Tuttle KR. New therapies for diabetic kidney disease. N Engl J Med. 2013;369:2549-2550.

3. Lewis EJ, Xu X. Abnormal glomerular permeability characteristics in diabetic nephropathy: implications for the therapeutic use of low-molecular weight heparin. Diabetes Care. 2008;31 Suppl 2:S202-207.
4. Meyer TW. Immunosuppression for diabetic glomerular disease? Kidney Int. 2003;63:377-378.
5. Mori Y, Ajay AK, Chang JH, Mou S, Zhao H, Kishi S, et al. KIM-1 mediates fatty acid uptake by renal tubular cells to promote progressive diabetic kidney disease. Cell Metab. 2021;33:1042-1061.e1047.
6. Vallon V, Thomson SC. The tubular hypothesis of nephron filtration and diabetic kidney disease. Nat Rev Nephrol. 2020;16:317-336.
7. Bagby SP. Diabetic nephropathy and proximal tubule ROS: challenging our glomerulocentricity. Kidney Int. 2007;71:1199-1202.
8. Li X, Yang W, Ma K, Zheng Z, Liu X, Hu B, et al. Circulating B Cell-Derived Small RNA Delivered by Extracellular Vesicles: A Dialogue Mechanism for Long-Range Targeted Renal Mitochondrial Injury in Obesity. Small. 2024;20:e2402526.
9. Li XQ, Xiao ZZ, Ma K, Liu XY, Liu HH, Hu B, et al. Angiotensin-Converting Enzyme-Dependent Intrarenal Angiotensin II Contributes to CTP: Phosphoethanolamine Cytidylyltransferase Downregulation, Mitochondrial Membranous Disruption, and Reactive Oxygen Species Overgeneration in Diabetic Tubulopathy. Antioxid Redox Signal. 2025;42:767-786.
10. Tsai YC, Dai CY, Tsai MJ, Hwang SJ, Yu PS, Hung WW, et al. Immune Cell Infiltration and Kynurenine Pathway Activation Define Early Injury and

753 Progression in Diabetic Nephropathy. Int J Biol Sci. 2026;22:1389-1406.
754 11. Miguel V, Shaw IW, Kramann R. Metabolism at the crossroads of inflammation
755 and fibrosis in chronic kidney disease. Nat Rev Nephrol. 2025;21:39-56.
756 12. Stamatiades EG, Tremblay ME, Bohm M, Crozet L, Bisht K, Kao D, et al. Immune
757 Monitoring of Trans-endothelial Transport by Kidney-Resident Macrophages.
758 Cell. 2016;166:991-1003.
759 13. Li J, Yang B, Pan T, Zhou X, Ma Z, Tang D, et al. BHLHE40 Orchestrates Effector
760 Tissue-Resident Memory CD8(+) T Cells and Limits Long-Term Survival of
761 Kidney Graft. Adv Sci (Weinh). 2026;13:e20518.
762 14. O'Brien KL, Finlay DK. Immunometabolism and natural killer cell responses. Nat
763 Rev Immunol. 2019;19:282-290.
764 15. Gong Z, Li Q, Shi J, Liu ET, Shultz LD, Ren G. Lipid-laden lung mesenchymal
765 cells foster breast cancer metastasis via metabolic reprogramming of tumor cells
766 and natural killer cells. Cell Metab. 2022;34:1960-1976.e1969.
767 16. Poznanski SM, Singh K, Ritchie TM, Aguiar JA, Fan IY, Portillo AL, et al.
768 Metabolic flexibility determines human NK cell functional fate in the tumor
769 microenvironment. Cell Metab. 2021;33:1205-1220.e1205.
770 17. Wang H, Cao K, Liu S, Xu Y, Tang L. Tim-3 Expression Causes NK Cell
771 Dysfunction in Type 2 Diabetes Patients. Front Immunol. 2022;13:852436.
772 18. Yoon Kim D, Kwon Lee J. Type 1 and 2 diabetes are associated with reduced
773 natural killer cell cytotoxicity. Cell Immunol. 2022;379:104578.
774 19. Horowitz A, Heeger P. Natural killer cells in kidney immune surveillance, injury

and fibrosis. Nat Rev Nephrol. 2026;22:215-228.

20. Law BMP, Wilkinson R, Wang X, Kildey K, Lindner M, Rist MJ, et al. Interferon-γ production by tubulointerstitial human CD56(bright) natural killer cells contributes to renal fibrosis and chronic kidney disease progression. Kidney Int. 2017;92:79-88.

21. Fu J, Sun Z, Wang X, Zhang T, Yuan W, Salem F, et al. The single-cell landscape of kidney immune cells reveals transcriptional heterogeneity in early diabetic kidney disease. Kidney Int. 2022;102:1291-1304.

22. Lampropoulou V, Sergushichev A, Bambouskova M, Nair S, Vincent EE, Loginicheva E, et al. Itaconate Links Inhibition of Succinate Dehydrogenase with Macrophage Metabolic Remodeling and Regulation of Inflammation. Cell Metab. 2016;24:158-166.

23. Cordes T, Wallace M, Michelucci A, Divakaruni AS, Sapcariu SC, Sousa C, et al. Immunoresponsive Gene 1 and Itaconate Inhibit Succinate Dehydrogenase to Modulate Intracellular Succinate Levels. J Biol Chem. 2016;291:14274-14284.

24. Mills EL, Ryan DG, Prag HA, Dikovskaya D, Menon D, Zaslona Z, et al. Itaconate is an anti-inflammatory metabolite that activates Nrf2 via alkylation of KEAP1. Nature. 2018;556:113-117.

25. Hooftman A, Angiari S, Hester S, Corcoran SE, Runtsch MC, Ling C, et al. The Immunomodulatory Metabolite Itaconate Modifies NLRP3 and Inhibits Inflammasome Activation. Cell Metab. 2020;32:468-478.e467.

26. Liao ST, Han C, Xu DQ, Fu XW, Wang JS, Kong LY. 4-Octyl itaconate inhibits

aerobic glycolysis by targeting GAPDH to exert anti-inflammatory effects. Nat Commun. 2019;10:5091.

27. Li W, Li Y, Kang J, Jiang H, Gong W, Chen L, et al. 4-octyl itaconate as a metabolite derivative inhibits inflammation via alkylation of STING. Cell Rep. 2023;42:112145.

28. Wculek SK. Jack-of-a-new-trade: Itaconate targets the PPP/G6PD to control lung cancer. Cell Metab. 2026;38:1264-1266.

29. Shan M, Zhang S, Luo Z, Deng S, Ran L, Zhou Q, et al. Itaconate promotes inflammatory responses in tissue-resident alveolar macrophages and exacerbates acute lung injury. Cell Metab. 2025;37:1750-1765.e1757.

30. Men Z, Lin Z, Wang Z, Tan P, Yu S, Ma X. Offense and defense: itaconate mediates bidirectional immune regulation of host-bacteria interaction. J Biomed Sci. 2026;33:68.

31. Willenbockel HF, Williams AT, Lucas A, Reynolds MB, Joulia E, Ruchhoeft ML, et al. In vivo itaconate tracing reveals degradation pathway and turnover kinetics. Nat Metab. 2025;7:1781-1790.

32. Natarajan SK, Lum J, Skeans JH, Nenwani M, Eyunni S, Mota M, et al. ZFTA-RELA ependymomas make itaconate to epigenetically drive fusion expression. Nature. 2026;652:1004-1015.

33. Xia S, Lin R, Jin L, Zhao L, Kang HB, Pan Y, et al. Prevention of Dietary-Fat-Fueled Ketogenesis Attenuates BRAF V600E Tumor Growth. Cell Metab. 2017;25:358-373.

34. Hervier B, Cremer I, Vieillard V. Polyfunctionality of bona fide resident lung CD69(+) natural killer cells. J Allergy Clin Immunol. 2017;140:317-318.
35. Horowitz NB, Mohammad IA, Shin JH, Hickey JW, Chockley P, Snyder G, et al. CD39(+)CD49a(+)CD103(+) cytotoxic tissue-resident natural killer cells infiltrate and control solid epithelial tumor growth in mice. Sci Transl Med. 2026;18:eadw5567.
36. Cooper GE, Mayall J, Donovan C, Haw TJ, Budden KF, Hansbro NG, et al. Antiviral Responses of Tissue-resident CD49a(+) Lung Natural Killer Cells Are Dysregulated in Chronic Obstructive Pulmonary Disease. Am J Respir Crit Care Med. 2023;207:553-565.
37. Wei H, Suo C, Gu X, Shen S, Lin K, Zhu C, et al. AKR1D1 suppresses liver cancer progression by promoting bile acid metabolism-mediated NK cell cytotoxicity. Cell Metab. 2025;37:1103-1118.e1107.
38. Wu S, Peng H, Li S, Huang L, Wang X, Li Y, et al. The ω-3 Polyunsaturated Fatty Acid Docosahexaenoic Acid Enhances NK-Cell Antitumor Effector Functions. Cancer immunol Res. 2024;12:744-758.
39. Turner JE, Rickassel C, Healy H, Kassianos AJ. Natural Killer Cells in Kidney Health and Disease. Front Immunol. 2019;10:587.
40. Hong S, Healy H, Kassianos AJ. The Emerging Role of Renal Tubular Epithelial Cells in the Immunological Pathophysiology of Lupus Nephritis. Front Immunol. 2020;11:578952.
41. Zhang ZX, Wang S, Huang X, Min WP, Sun H, Liu W, et al. NK cells induce

apoptosis in tubular epithelial cells and contribute to renal ischemia-reperfusion injury. J Immunol. 2008;181:7489-7498.

42. Mansouri S, Hesami G, Ambikan A, Karger A, Klatt S, Neogi U, et al. IRG1/itaconate rewires macrophage and lung tumor metabolism through G6PD inhibition. Cell Metab. 2026;38:1460-1477.e1468.

43. Watermann P, Kalsi GK, Dringen R, Arend C. Differential Effects of Itaconate and its Esters on the Glutathione and Glucose Metabolism of Cultured Primary Rat Astrocytes. Neurochem Res. 2024;50:24.

44. Hu S, Balakrishnan A, Bok RA, Anderton B, Larson PE, Nelson SJ, et al. 13C-pyruvate imaging reveals alterations in glycolysis that precede c-Myc-induced tumor formation and regression. Cell Metab. 2011;14:131-142.

45. Lee KM, Giltnane JM, Balko JM, Schwarz LJ, Guerrero-Zotano AL, Hutchinson KE, et al. MYC and MCL1 Cooperatively Promote Chemotherapy-Resistant Breast Cancer Stem Cells via Regulation of Mitochondrial Oxidative Phosphorylation. Cell Metab. 2017;26:633-647.e637.

46. Swain A, Bambouskova M, Kim H, Andhey PS, Duncan D, Auclair K, et al. Comparative evaluation of itaconate and its derivatives reveals divergent inflammasome and type I interferon regulation in macrophages. Nat Metab. 2020;2:594-602.

47. Gao H, Ding M, Liu Y, Wang Y, Zhao S, Chen J, et al. Reprogramming immunity with itaconate: metabolic mechanisms and therapeutic perspectives. Inflamm Res. 2025;74:128.

48. Xie Y, Cheng Q, Xu ML, Xue J, Wu H, Du Y. Itaconate: A Potential Therapeutic Strategy for Autoimmune Disease. Scand J Immunol. 2025;101:e70026.
49. Kang M, Tang D, Huang W, Zhou M, Ma Q, Lan Y, et al. Emerging role of Itaconate in inflammatory bowel disease: From multitarget Immunometabolic mechanisms to therapeutic translation. Int Immunopharmacol. 2025;166:115632.
50. Cheng C, Zhang Q, Li Y, Jiang J, Xie L, Shen H, et al. Interplay Between Liver Type 1 Innate Lymphoid Cells and NK Cells Drives the Development of Alcoholic Steatohepatitis. Cell Mol Gastroenterol Hepatol. 2023;15:261-274.
51. Fuchs A, Vermi W, Lee JS, Lonardi S, Gilfillan S, Newberry RD, et al. Intraepithelial type 1 innate lymphoid cells are a unique subset of IL-12- and IL-15-responsive IFN-γ-producing cells. Immunity. 2013;38:769-781.
52. Turner JE, Becker M, Mittrücker HW, Panzer U. Tissue-Resident Lymphocytes in the Kidney. J Am Soc Nephrol. 2018;29:389-399.
53. Thompson CB, Vousden KH, Johnson RS, Koppenol WH, Sies H, Lu Z, et al. A century of the Warburg effect. Nat Metab. 2023;5:1840-1843.
54. Wang Y, Patti GJ. The Warburg effect: a signature of mitochondrial overload. Trends Cell Biol. 2023;33:1014-1020.
55. Zhang ZX, Shek K, Wang S, Huang X, Lau A, Yin Z, et al. Osteopontin expressed in tubular epithelial cells regulates NK cell-mediated kidney ischemia reperfusion injury. J Immunol. 2010;185:967-973.
56. Xie A, Brunner JS, Chakraborty S, Montero AM, Bridgeman AE, Paras KI, et al. Citrate clearance is a major function of aconitase 2 in the canonical TCA cycle.

Cell. 2026;189:2684-2699.e2621.

57. Shan C, Elf S, Ji Q, Kang HB, Zhou L, Hitosugi T, et al. Lysine acetylation activates 6-phosphogluconate dehydrogenase to promote tumor growth. Mol Cell. 2014;55:552-565.

58. Lin R, Elf S, Shan C, Kang HB, Ji Q, Zhou L, et al. 6-Phosphogluconate dehydrogenase links oxidative PPP, lipogenesis and tumour growth by inhibiting LKB1-AMPK signalling. Nat Cell Biol. 2015;17:1484-1496.

59. Elia I, Rowe JH, Johnson S, Joshi S, Notarangelo G, Kurmi K, et al. Tumor cells dictate anti-tumor immune responses by altering pyruvate utilization and succinate signaling in CD8(+) T cells. Cell Metab. 2022;34:1137-1150.e1136.

60. Strelko CL, Lu W, Dufort FJ, Seyfried TN, Chiles TC, Rabinowitz JD, et al. Itaconic acid is a mammalian metabolite induced during macrophage activation. J Am Chem Soc. 2011;133:16386-16389.

61. Palmieri EM, Gonzalez-Cotto M, Baseler WA, Davies LC, Ghesquière B, Maio N, et al. Nitric oxide orchestrates metabolic rewiring in M1 macrophages by targeting aconitase 2 and pyruvate dehydrogenase. Nat Commun. 2020;11:698.

62. Del Prado L, Jaraíz-Rodríguez M, Agro M, Zamora-Dorta M, Azpiazu N, Calleja M, et al. Compensatory activity of the PC-ME1 metabolic axis underlies differential sensitivity to mitochondrial complex I inhibition. Nat Commun. 2024;15:8682.

63. Zeng QG, Li L, Chang T, Sun Y, Zheng B, Xue LN, et al. Phosphorylation of POU3F3 Mediated Nuclear Translocation Promotes Proliferation in Non-Small

Cell Lung Cancer through Accelerating ATP5PF Transcription and ATP Production. Adv Sci (Weinh). 2025;12:e2411503.

64. Khameneh HJ, Fonta N, Zenobi A, Niogret C, Ventura P, Guerra C, et al. Myc controls NK cell development, IL-15-driven expansion, and translational machinery. Life Sci Alliance. 2023;6:e202302069.

65. Yang P, Wang W, Liu Q, Mu S, Zha Y, Yan W, et al. Metabolic reprogramming of NK cells drives anti-tumor immunity. Crit Rev Oncol Hematol. 2025;215:104859.

66. Loftus RM, Assmann N, Kedia-Mehta N, O'Brien KL, Garcia A, Gillespie C, et al. Amino acid-dependent cMyc expression is essential for NK cell metabolic and functional responses in mice. Nat Commun. 2018;9:2341.

67. KDOQI Clinical Practice Guidelines and Clinical Practice Recommendations for Diabetes and Chronic Kidney Disease. Am J Kidney Dis. 2007;49:S12-154.

68. Expert consensus on the diagnosis and management of diabetic kidney disease. Chin Med J (Engl.). 2020;133:2333-2334.

69. Tervaert TW, Mooyaart AL, Amann K, Cohen AH, Cook HT, Drachenberg CB, et al. Pathologic classification of diabetic nephropathy. J Am Soc Nephrol. 2010;21:556-563.

70. Sun P, Xu X, Hu B, Zhang K, Khan A, Chen H, et al. Targeting NK cell CLEC12B enhances cancer immunotherapy. Nat Immunol. 2026;27:985-999.

71. Yamada Y, Nakashima A, Doi S, Ishiuchi N, Kanai R, Miyasako K, et al. Localization and Maintenance of Engrafted Mesenchymal Stem Cells Administered via Renal Artery in Kidneys with Ischemia-Reperfusion Injury. Int

J Mol Sci. 2021;22:4178.

72. Wu L, Liu C, Chang DY, Zhan R, Sun J, Cui SH, et al. Annexin A1 alleviates kidney injury by promoting the resolution of inflammation in diabetic nephropathy. Kidney Int. 2021;100:107-121.

73. Li ZH, Fang L, Wu L, Chang DY, Dong M, Ji L, et al. ANXA1 improves mitochondrial homeostasis through uncoupling protein 1 in diabetic nephropathy. J Adv Res. 2026;86:689-708.

74. Jin WN, Shi K, He W, Sun JH, Van Kaer L, Shi FD, et al. Neuroblast senescence in the aged brain augments natural killer cell cytotoxicity leading to impaired neurogenesis and cognition. Nat Neurosci. 2021;24:61-73.

75. Zhang J, Han C, Dai H, Hou J, Dong Y, Cui X, et al. Hypoxia-Inducible Factor-2α Limits Natural Killer T Cell Cytotoxicity in Renal Ischemia/Reperfusion Injury. J Am Soc Nephrol. 2016;27:92-106.

76. Zhang L, Norberg SM, Karimipour F, Davies JS, Kuznetsov A, Lassoued W, et al. Adoptive transfer of membrane-restricted IL-12-TCR T cells promotes antigen spreading and elimination of antigen-negative tumor variants. J Immunother Cancer. 2024;12:e009868.

77. Zhang H, Chen T, Ren J, Xia Y, Onuma A, Wang Y, et al. Pre-operative exercise therapy triggers anti-inflammatory trained immunity of Kupffer cells through metabolic reprogramming. Nat Metab. 2021;3:843-858.

78. Zhang S, Yue T, Jin P, Zhang X, Huo Q, Li W, et al. 4-Octyl itaconate attenuates radiation-induced intestinal injury associated with ferroptosis inhibition and

951 microbiota rebalance. Free Radic Biol Med. 2026;250:386-398.
952 79. Zhong Z, Wang S, Ren Q, Jiao X, Xu L, Dong X, et al. Stromal cell-derived
953 itaconate promotes endometriosis via macrophage NRF2 and lysosomal pH
954 modulation. Redox Biol. 2026;92:104101.
955 80. Chen Z, Wang B, Zheng J, Liu C, Xu P, Zhou Q, et al. Reprogramming tumor-
956 associated macrophages and blocking PD-L1 via engineered outer membrane
957 vesicles to enhance T cell infiltration and cytotoxic functions. J
958 Nanobiotechnology. 2025;23:514.
959 81. Matsumoto A, Kinoshita M, Ono S, Tsujimoto H, Majima T, Habu Y, et al.
960 Cooperative IFN-gamma production of mouse liver B cells and natural killer cells
961 stimulated with lipopolysaccharide. J Hepatol. 2006;45:290-298.
962 82. Wang F, Zhang G, Xu T, Ma J, Wang J, Liu S, et al. High and selective cytotoxicity
963 of ex vivo expanded allogeneic human natural killer cells from peripheral blood
964 against bladder cancer: implications for natural killer cell instillation after
965 transurethral resection of bladder tumor. J Exp Clin Cancer Res. 2024;43:24.
966 83. Wang F, Zhang X, Liu W, Zhou Y, Wei W, Liu D, et al. Activated Natural Killer
967 Cell Promotes Nonalcoholic Steatohepatitis Through Mediating JAK/STAT
968 Pathway. Cell Mol Gastroenterol Hepatol. 2022;13:257-274.
969 84. Howard C, Tao S, Yang HC, Fogo AB, Woodgett JR, Harris RC, et al. Specific
970 deletion of glycogen synthase kinase-3β in the renal proximal tubule protects
971 against acute nephrotoxic injury in mice. Kidney Int. 2012;82:1000-1009.
972 85. Yang W, Jia M, Zhou F, Zhang M, Qu S, Zeng C, et al. Renal tubular VMP1

protects against acute kidney injury via modulating autophagy and autophagy-independent pathway. Autophagy. 2025;21:2792-2808.

Acknowledgements

The authors acknowledge the patients for allowing the use of their biopsy data for research purposes. This work was supported by the National Natural Science Foundation of China (82270756), National Natural Science Foundation of China (82601395), Guangdong Basic and Applied Basic Research Foundation (2024A1515011405); Guangdong Engineering Technology Research Center (507204531040), Guangzhou Development Zone Entrepreneurship Leading Talent Project (2017-L153), Guangzhou Entrepreneurship Leading Team (202009030005), Heyuan City Science and Technology Plan Project (230510171473347), Heyuan City Science and Technology Plan Project (230510171473346).

Author contributions

Conceptualization, Y.M., F.J., and L.H.Y.; methodology, X.Q.L., Lei. L., and X.Y.L.; validation, Lei. L., X.Q.L., and X.Y.L.; formal analysis, X.Q.L., S.T.Z, K.M., M.Y.X., H.H.L., H.Y.L., Le. L., and B.H.; investigation, Lei. L., X.Y.L., F.J., L.H.Y., H.H.L., H.Y.L., Le. L., B.H., and M.Y.X.; resources, Y.M., L.H.Y., and F.J. ; data curation, X.Q.L., Lei. L., X.Y.L., S.T.Z, and K.M.; writing – original draft, X.Q.L., Lei. L., and X.Y.L.; writing – revision & editing, all authors; visualization, X.Q.L., Lei. L., X.Y.L., F.J., and Y.M.; supervision, Y.M., F.J., and L.H.Y.; project administration, Y.M. and F.J.; funding acquisition, Y.M., F.J., and L.H.Y.

Competing interests

The authors declare no competing interests.

Correspondence and requests for materials should be addressed to Yu Meng.

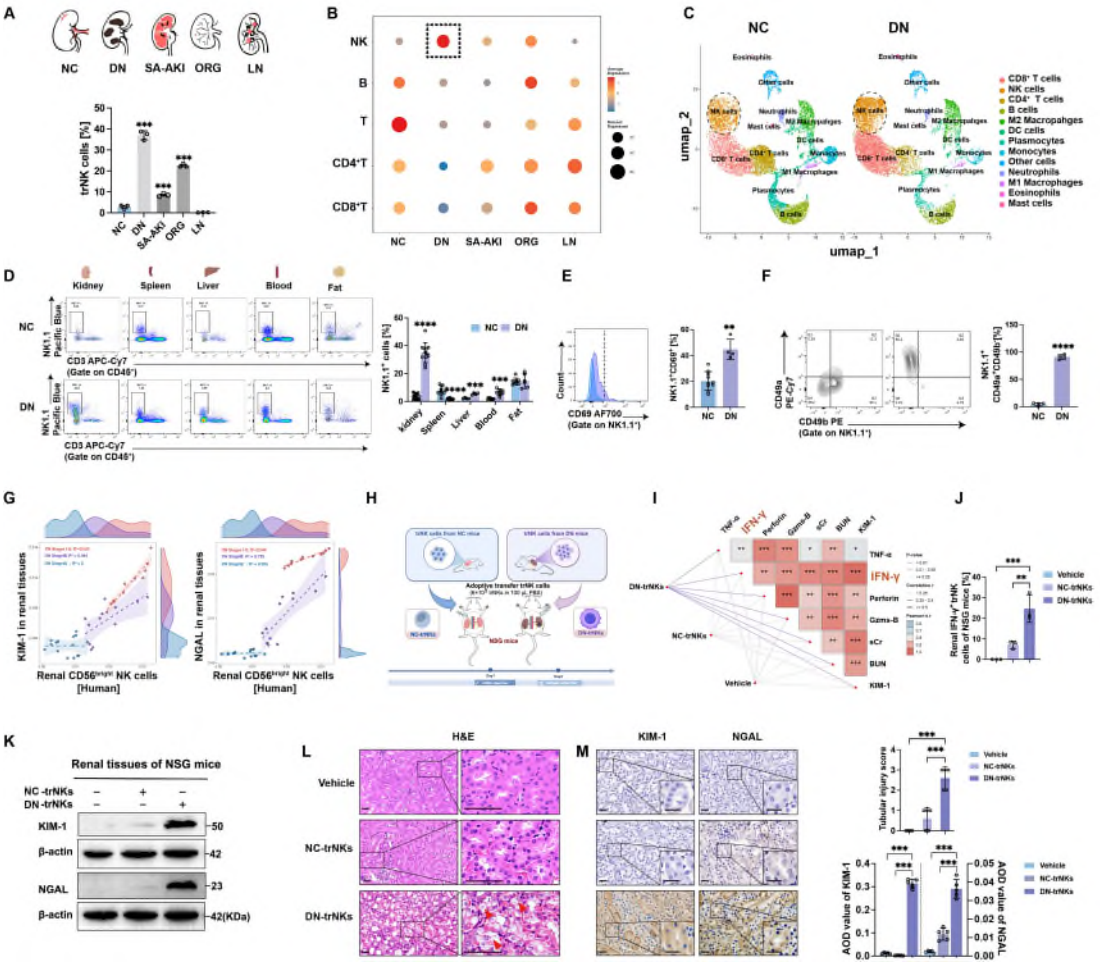


Fig. 1. Expansion of renal tissue resident NK cells (trNKs) exacerbates tubular injury in diabetic nephropathy (DN).

(A) Flow cytometry of renal trNKs proportion in different kidney disease models, revealing a marked expansion of trNKs in DN.

(B) Heatmap showing the relative proportions of trNKs, B cells and T cells ($CD4^+$ T and $CD8^+$ T cells) in different kidney disease models.

(C) UMAP plot of renal cells from publicly available single-cell RNA sequencing (scRNAseq) datasets of normal control (NC) and DN mice.

(D) Flow cytometry of trNKs proportion in the kidney, spleen, liver, blood, and fat from NC and DN mice. Renal trNKs are markedly increased in DN mice.

(E and F) Flow cytometric identification of renal trNKs as NK1.1^{+}CD49a^{+}CD69^{+}CD49b^{-}, consistent with a tissue-resident phenotype.

(G) Correlation analysis showing the positive relationship between IHC-AOD values of renal CD56^{bright} NK cells and tubular injury biomarker (KIM-1 and NGAL) in DN patients. Pearson's correlation coefficient (*r*) and *P* values are shown; IHC, immunohistochemistry; AOD, average optical density; KIM-1, kidney injury molecule-1; NGAL, neutrophil gelatinase-associated lipocalin (n = 11 patients).

(H) Schematic of adoptive transfer of trNKs into NOD-scid IL2Rγ$^{-/-}$ (NSG) mice via intrarenal arterial injection. Mice receive vehicle, NC-derived trNKs (NC-trNKs), or DN-derived trNKs (DN-trNKs) (n=3 per group).

(I) Correlation heatmap showing the positive relationships among trNKs inflammatory/cytotoxic mediators [IFN-γ (the most significant), TNF-α, granzyme B and perforin], renal function parameters (sCr and BUN) and urinary KIM-1 level in NSG mice. Pearson's correlation coefficients are color-coded, and line thickness indicates significance level. IFN-γ, interferon-γ; TNF-α, tumor necrosis factor-α; sCr, serum creatinine; BUN, blood urea nitrogen.

(J) Flow cytometry revealing the increased IFN-γ^{+} trNKs proportion in NSG mice adoptively transferred with DN-trNKs.

(K) Western blot confirming DN-trNKs directly increases KIM-1 and NGAL protein levels in renal tissues from the NSG mice.

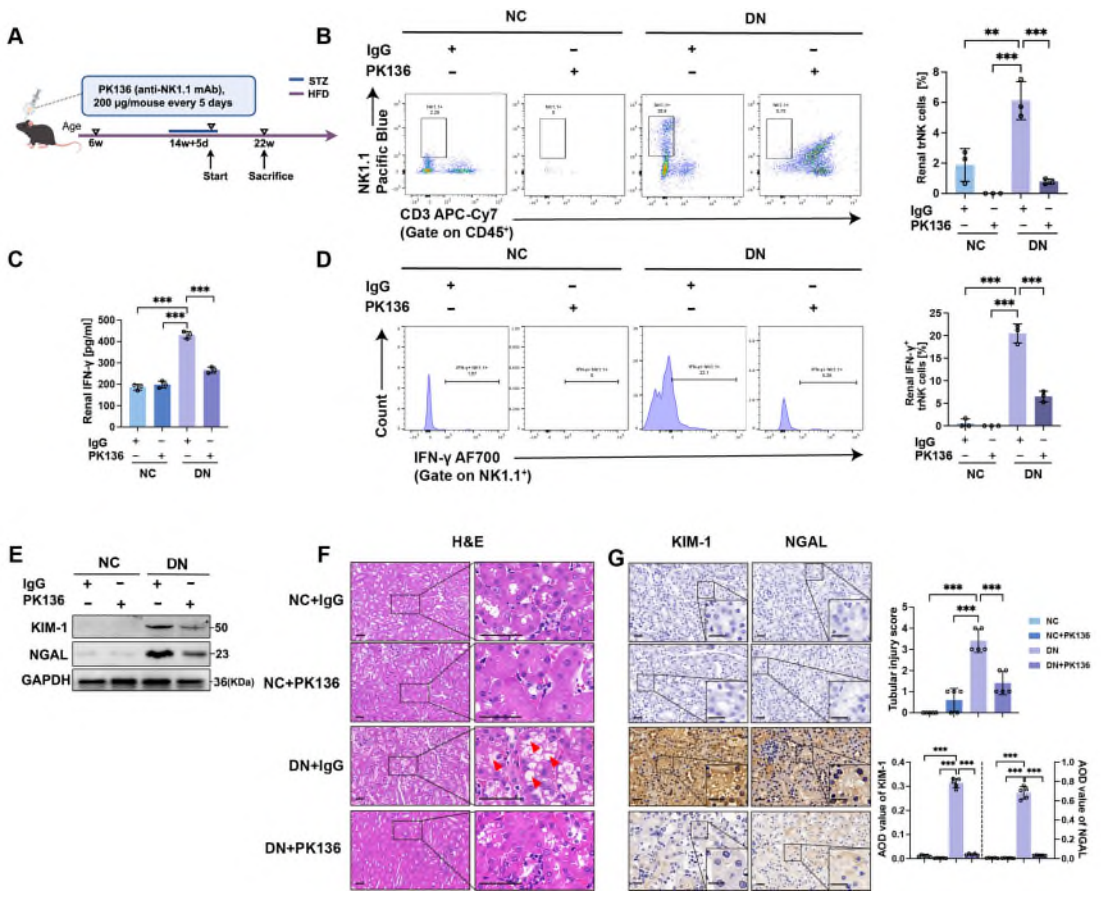


Fig. 2. NK cell depletion ameliorates tubular injury in DN.

(A) Schematic of *in vivo* administration of PK136 (anti-NK1.1 monoclonal antibody) via the inner canthus veniplex into NC and DN mice (n=3 per group).

(B) Flow cytometry analysis of renal trNKs, confirming the efficacy of NK cell depletion in PK136-treated NC and DN mice.

(C) Enzyme-linked immunosorbent assay (ELISA) revealing decreased IFN-γ levels in renal tissues from PK136-treated NC and DN mice.

(D) Flow cytometry further confirming decreased IFN-γ^+ trNKs proportion in PK136-treated NC and DN mice.

(E) Western blot showing decreased KIM-1 and NGAL protein levels in renal tissues of DN mice after NK cell depletion (PK136 treatment).

(F) Representative H&E images and tubular injury scores in renal cortex sections from PK136-treated NC and DN mice. Red arrow, vacuolization. Scale bars, 25-100 μm. (G) Representative IHC images and quantification of KIM-1 and NGAL in renal cortex sections from PK136-treated NC and DN mice. Scale bars, 25-50 μm.

Data are presented as mean ± SD. Two-way ANOVA with Tukey's post hoc test for (B, C, D, F and G). *p<0.05, **p<0.01, ***p<0.001, ****p<0.0001. ns indicates no significance.

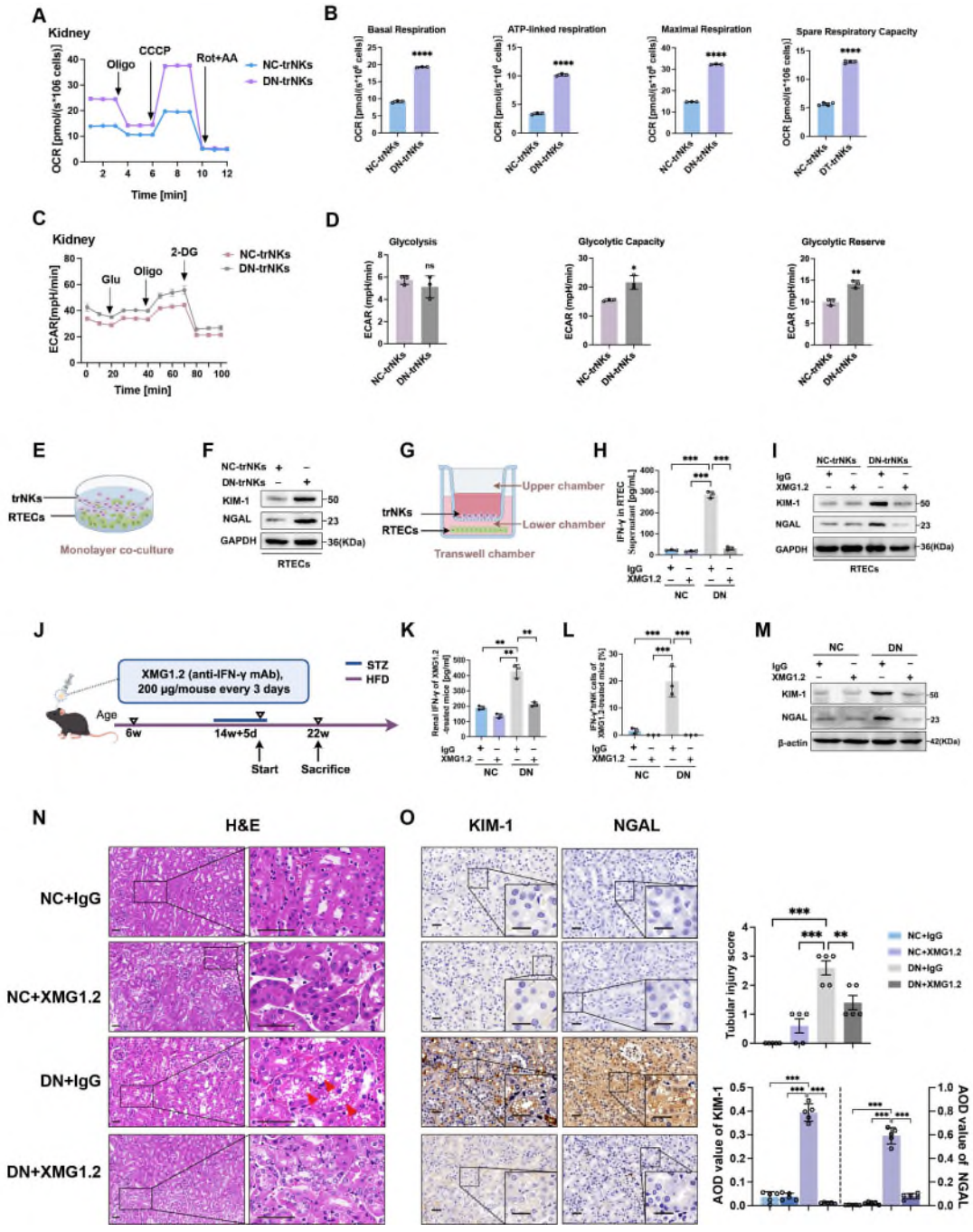


Fig. 3. Co-enhanced oxidative phosphorylation (OXPHOS) and glycolysis in renal DN-trNKs and IFN-γ-mediated pro-inflammatory tubular injury.

(A) Elevated oxygen consumption rate (OCR) for mitochondrial respiration in DN-trNKs.

(B) OCR-derived bioenergetic parameters (basal respiration, ATP production, maximal respiration and spare respiratory capacity).

(C) Elevated extracellular acidification rate (ECAR) for glycolysis in DN-trNKs.

(D) ECAR-derived bioenergetic parameters (glycolysis, glycolytic capacity, and glycolytic reserve).

(E) Schematic of direct-contact monolayer co-culture of trNKs and renal tubular epithelial cells (RTECs).

(F) Western blot showing increased KIM-1 and NGAL protein levels of RTECs directly co-cultured with DN-trNKs *in vitro*.

(G) Schematic of a Transwell co-culture system to evaluate the paracrine effects of trNKs on RTECs.

(H) ELISA revealing increased IFN-γ level in the supernatant of RTECs co-cultured with DN-trNKs, which is neutralized by XMG1.2 (IFN-γ neutralizing monoclonal antibody).

(I) Western blot showing increased KIM-1 and NGAL protein levels in RTECs co-cultured with DN-trNKs in a Transwell system, which are reduced by XMG1.2 *in vitro*.

(J) Schematic of *in vivo* XMG1.2 administration via the inner canthus veniplex into NC and DN mice (n=3 per group).

(K) ELISA revealing increased IFN-γ level in renal tissues of DN mice, which is neutralized by XMG1.2.

(L) Flow cytometry further confirming increased IFN-γ^+ trNKs proportion in DN mice, which is reduced by XMG1.2.

(M) Western blot showing increased KIM-1 and NGAL protein levels in renal tissues from the DN mice, which are reduced by XMG1.2.

(N) Representative H&E images and tubular injury scores of renal cortex sections from XMG1.2-treated NC and DN mice. Red arrow, vacuolization. Scale bars, 25-100 μm.

(O) Representative IHC images and quantification of KIM-1 and NGAL in renal cortex sections from the XMG1.2-treated NC and DN mice. Scale bars, 25-50 μm.

Data are presented as mean ± SD. Two-tailed unpaired Student's t test for (A-D), and two-way ANOVA with Tukey's post hoc test for (H, K, L, N and O). *p<0.05, **p<0.01, ***p<0.001, ****p<0.0001.

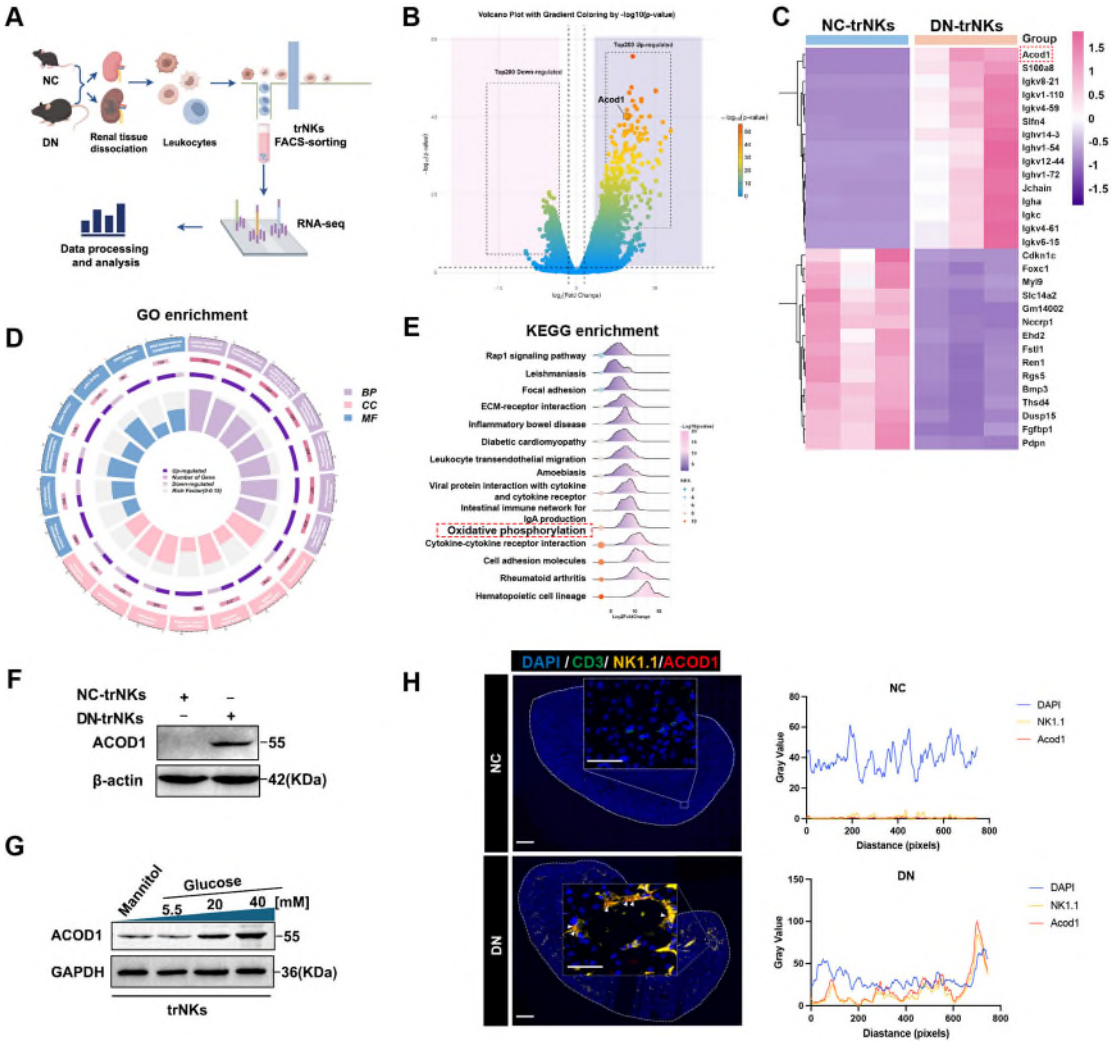


Fig. 4. Aconitate decarboxylase 1 (ACOD1) upregulation and OXPHOS enrichment in DN-trNKs.

(A) Schematic of fluorescence-activated cell sorting (FACS)-sorted NC- and DN-trNKs, followed by RNA-sequencing (RNA-seq) analysis (n=150-180 mice).

(B) Volcano plot of differentially expressed genes (DEGs) between NC- and DN-trNKs. Significantly upregulated (pink, n = 200) and downregulated (purple, n = 200) genes are shown (adjusted $p < 0.05$, $|\log_2 FC| > 1$). Acod1 is labeled.

(C) Heatmap of top 15 significant DEGs with upregulated genes (pink) and downregulated genes (purple). Acod1 is the top-ranked upregulated gene among DEGs in DN-trNKs.

(D) Gene Ontology (GO) enrichment analysis of DEGs. GO terms are categorized into biological process (BP, purple), cellular component (CC, pink), and molecular function (MF, blue). Immune/lymphocyte-related biological processes are highlighted.

(E) Kyoto Encyclopedia of Genes and Genomes (KEGG) enrichment analysis of top 15 pathways. OXPHOS ranks among the top five enriched pathways. Color, P-value; size, gene count.

(F) Western blot confirming the increased ACOD1 protein level in DN-trNKs.

(G) Western blot of ACOD1 in trNKs exposed to mannitol (osmolarity control), normal glucose (NG, 5.5 mM), moderate glucose (MG, 20 mM), and high glucose (HG, 40 mM).

(H) Representative immunofluorescence (IF) co-staining images and fluorescence intensity of CD3 (green), NK1.1 (yellow) and ACOD1 (red) in renal cortex sections from NC and DN mice. Nuclei are counterstained with DAPI (blue). Scale bars, 10-500 μm.

Data are presented as mean ± SD. Two-tailed unpaired Student's t test for (B and C). *p<0.05, **p<0.01, ***p<0.001, ****p<0.0001.

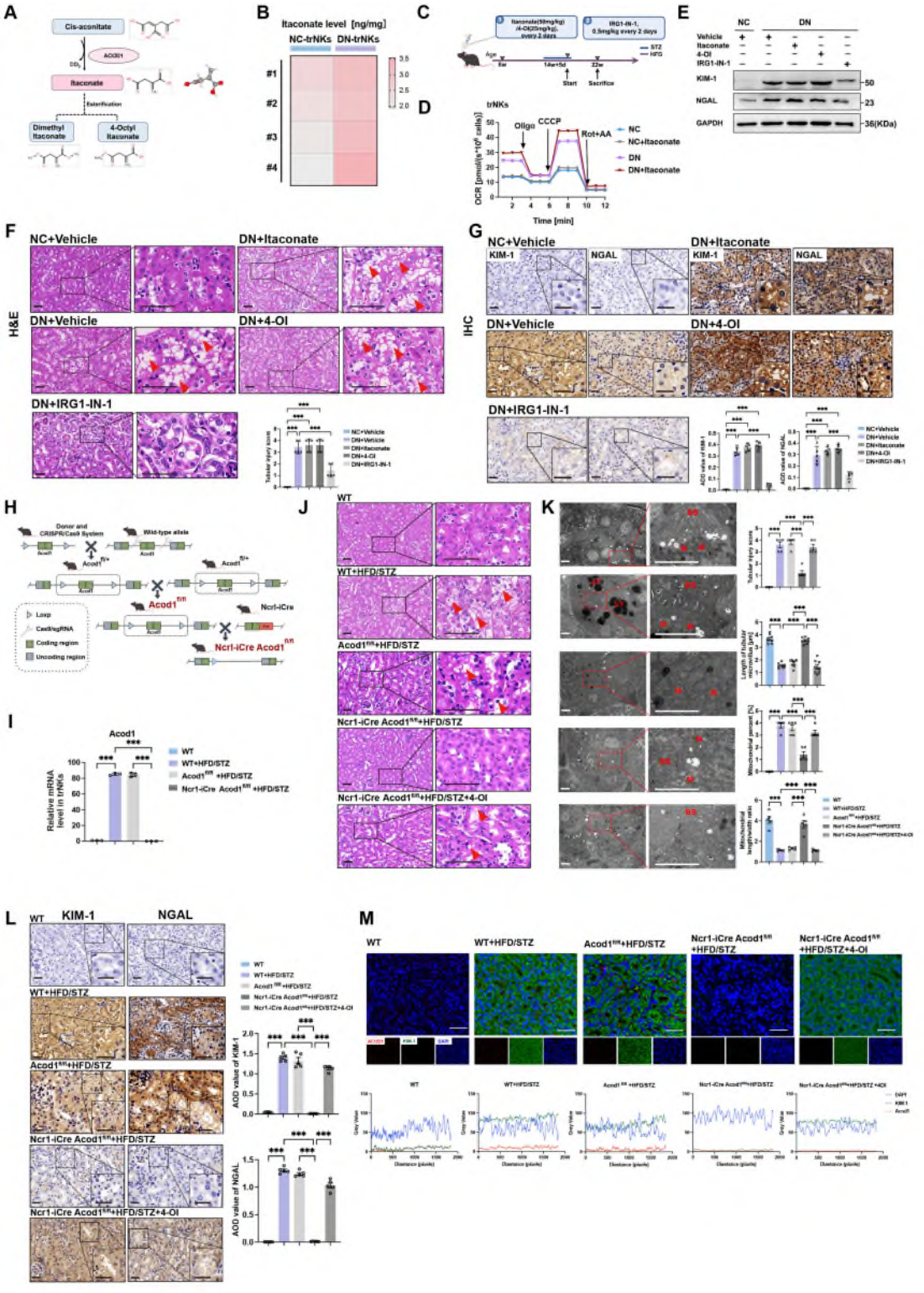


Fig. 5. Itaconate exacerbates tubular injury, while NK cell-specific Acod1 knockout alleviates DN.

(A) Schematic of the itaconate biosynthetic pathway. In the tricarboxylic acid (TCA)

cycle, cis-aconitate is converted to itaconate via the enzyme ACOD1. Itaconate is subsequently esterified to cell permeable derivatives, including dimethyl itaconate and 4-octyl-itaconate (4-OI).

(B) ELISA revealing the increased itaconate levels in DN-trNKs compared with NC-trNKs.

(C) Schematic of *in vivo* administration of itaconate/4-OI and IRG1-IN-1 (ACOD1 inhibitor) via the inner canthus veniplex in NC and DN mice (n=3 per group).

(D) Elevated OCR and corresponding bioenergetic parameters for DN-trNKs, which are exaggerated by itaconate treatment.

(E) Western blot showing increased KIM-1 and NGAL protein levels in renal tissues from mice treated with itaconate/4-OI, which are reduced by IRG1-IN-1.

(F) Representative H&E images and tubular injury scores in renal cortex sections from mice treated with itaconate/4-OI or IRG1-IN-1. Red arrow, vacuolization. Scale bars, 25-100 μm.

(G) Representative IHC images and quantification of KIM-1 and NGAL in renal cortex sections from mice treated with itaconate/4-OI-or IRG1-IN-1. Red arrow, vacuolization. Scale bars, 25-50 μm.

(H) Schematic of *in vivo* NK cell-specific Acod1 knockout. $Acod1^{flox/flox}$ ($Acod1^{fl/fl}$, n=12) mice are crossed with Ncr1-iCre mice to generate NK cell-specific Acod1 knockout mice (*Ncr1-iCre* $Acod1^{fl/fl}$, n=14). Both genotypes underwent high-fat diet (HFD) / streptozotocin (STZ)-DN induction, with a subset receiving 4-OI treatment (n=3).

(I) Reverse transcription quantitative polymerase chain reaction (RT-qPCR) validation of Acod1 knockout efficacy. Acod1 mRNA levels are undetectable in trNKs from *Ncr1-iCre Acod1* $^{fl/fl}$ mice.

(J) Representative H&E images and tubular injury scores for WT (NC), WT+HFD/STZ (DN), *Acod1*$^{fl/fl}$ + HFD/STZ, *Ncr1-iCre Acod1*$^{fl/fl}$ + HFD/STZ and *Ncr1-iCre Acod1*$^{fl/fl}$ + HFD/STZ+4-OI mice. Red arrow, vacuolization. Scale bars, 25-100 μm.

(K) Representative images of transmission electron microscopy (TEM) and quantitative results (tubular microvillus, mitochondrial percentage, and mitochondrial length/width ratio) of the indicated genotypes. M, mitochondria; BB, Brush border; LY, lysosome. Scale bars, 2-10 μm.

(L) Representative IHC images and quantification of KIM-1 and NGAL in renal cortex sections from the indicated genotypes. Scale bars, 25-50 μm.

(M) Representative IF co-staining images and fluorescence intensity of ACOD1 (red) and KIM-1 (green) in renal cortex sections from the indicated genotypes. Nuclei are counterstained with DAPI (blue). Scale barss, 20 μm.

Data are presented as mean ± SD. Two-way ANOVA with Tukey's post hoc test for (F, G, and I-L). *p<0.05, **p<0.01, ***p<0.001, ****p<0.0001.

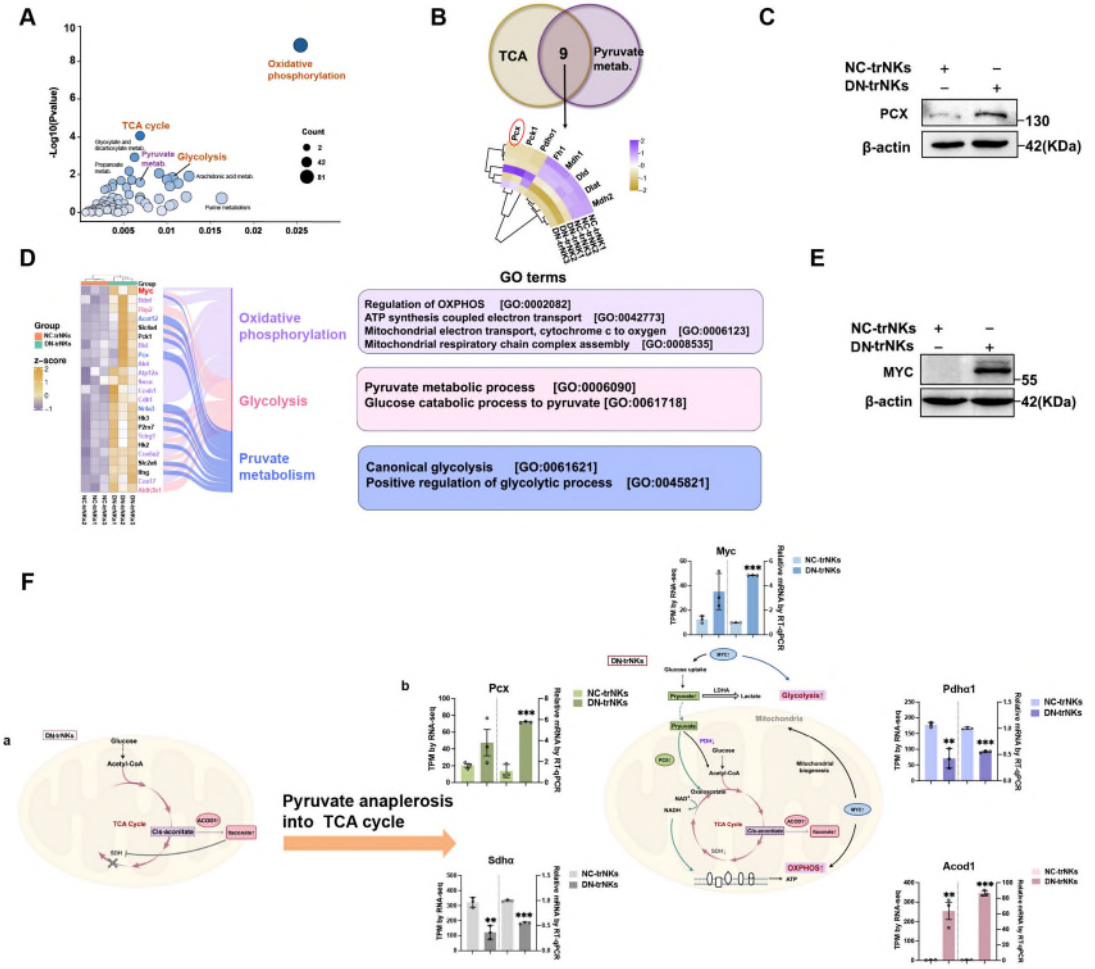


Fig. 6. Pyruvate carboxylase (Pcx)-mediated TCA anaplerosis and myelocytomatosis oncogene (Myc)-driven transcriptional reprogramming in DN-trNKs.

(A) Enrichment analysis of upregulated metabolic pathways in DN-trNKs. Significantly enriched pathways include OXPHOS, glycolysis, pyruvate metabolism, and the TCA cycle.

(B) Venn diagram depicting the overlap of upregulated DEGs enriched in TCA cycle and pyruvate metabolism pathways. Pcx is identified as the top-ranked candidate among the nine overlapping genes.

(C) Western blot confirming increased PCX protein level in DN-trNKs compared with NC-trNKs.

(D) Sankey diagram identifying Myc as an overlapping regulator at the intersection of the OXPHOS (purple)-glycolysis (pink)-pyruvate(blue). GO terms related to these metabolic processes are shown.

(E) Western blot confirming increased MYC protein level in DN-trNKs compared with NC-trNKs.

(F) Schematic of the proposed immunometabolic reprogramming of DN-trNKs. (a) ACOD1-catalyzed itaconate production blocks TCA by inhibiting succinate dehydrogenase (SDH). (b) Pyruvate dehydrogenase (PDH) downregulation accumulates pyruvate for PCX-mediated anaplerosis to replenish TCA intermediates, while MYC co-activates OXPHOS and glycolysis. RNA-seq and RT-qPCR confirming the elevated mRNA levels of Acod1, Pcx, Myc, alongside the downregulation of Pdhα1and Sdhα in DN-trNKs. Pdhα1, pyruvate dehydrogenase E1 alpha 1 subunit; Sdhα, succinate dehydrogenase complex subunit A.

Data are presented as mean ± SD. Two-tailed unpaired Student's t test for (F). *$p<0.05$, **$p<0.01$, ***$p<0.001$.

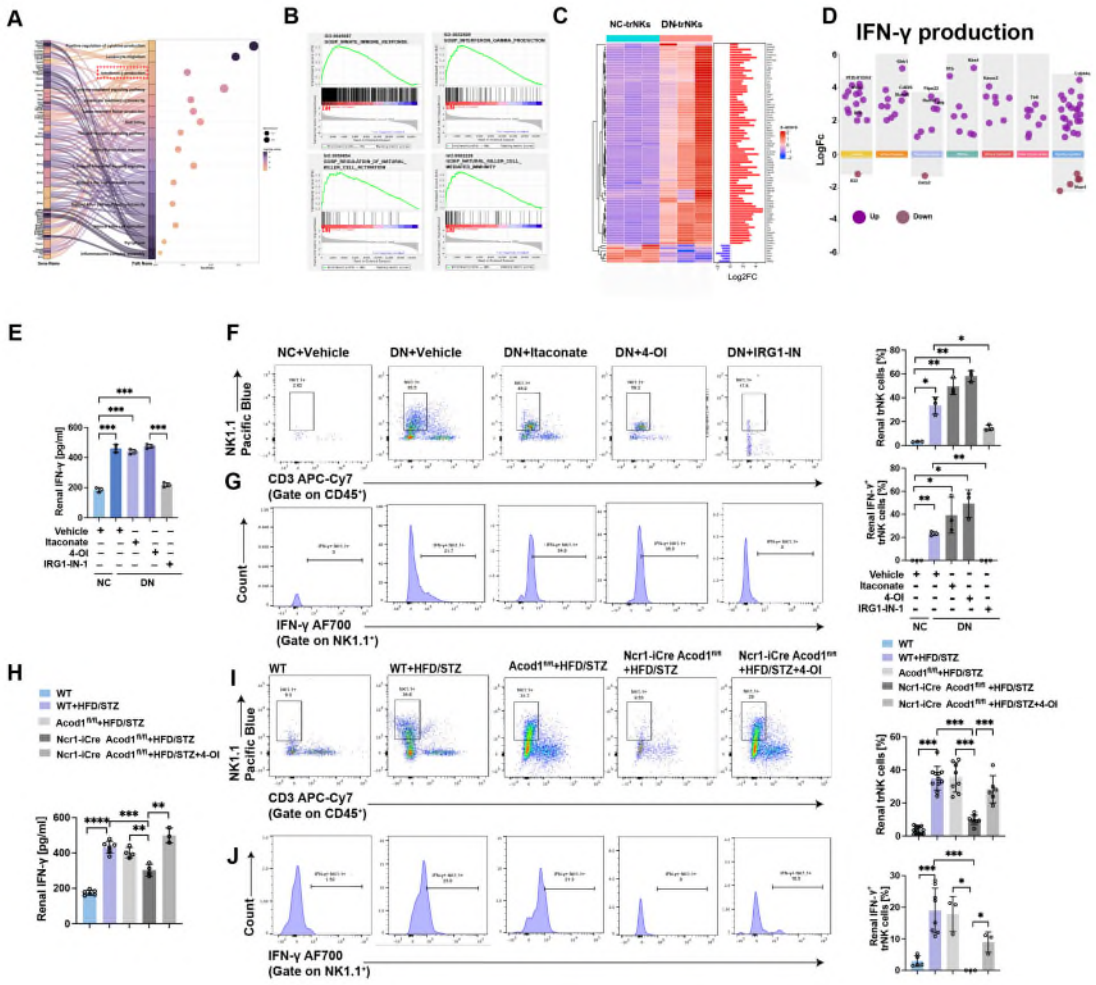


Fig. 7. Itaconate promotes, whereas NK cell-specific Acod1 knockdown suppresses, IFN-γ production from DN-trNKs.

(A) Sankey diagram of inflammation related pathways in DN-trNKs, highlighting significant enrichment of IFN-γ production pathway.

(B) Gene Set Enrichment Analysis (GSEA) showing DN-trNKs are enriched for innate immune response, IFN-γ production, NK cell activation, and NK cell-mediated immunity.

(C and D) Heatmap of IFN-γ-associated genes upregulated in DN-trNKs (C), categorized into cytokines, surface receptors, transcription factors, effectors, immune checkpoint, innate immune sensors, and signaling regulators (D).

(E) ELISA revealing increased IFN-γ level in renal tissues from the mice treated with itaconate/4-OI, which is reduced by IRG1-IN-1.

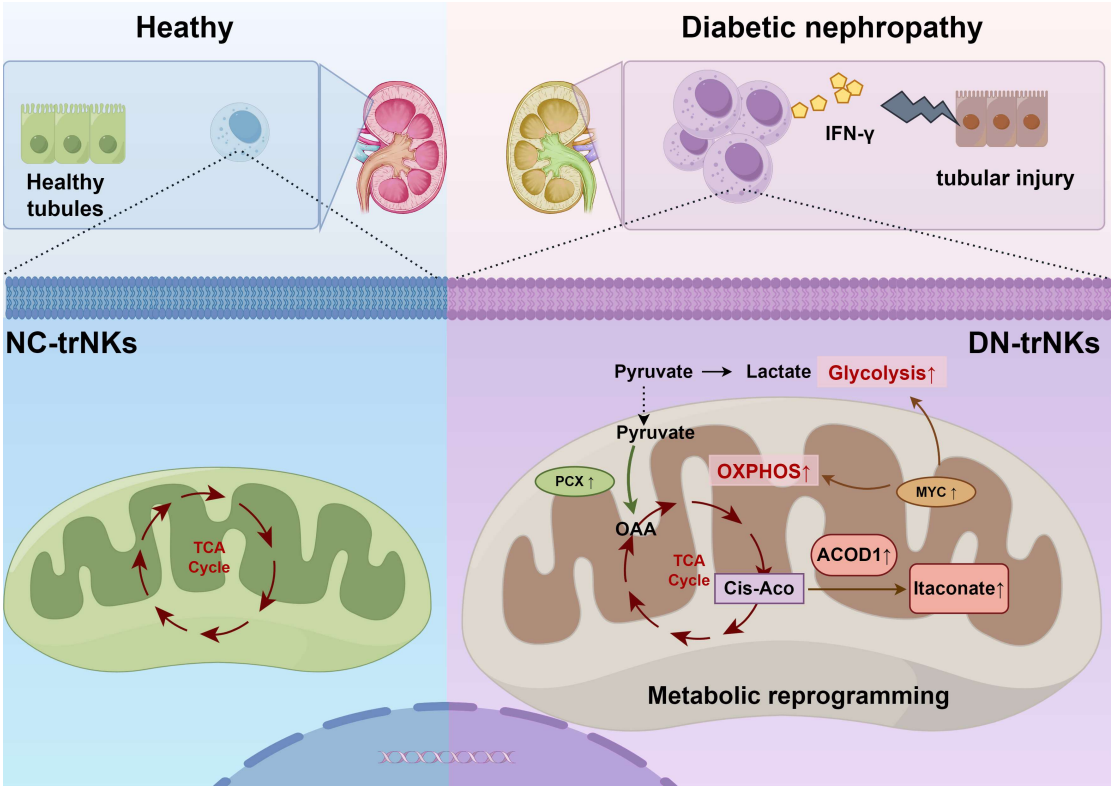
(F and G) Flow cytometry revealing increased proportions of trNKs (F) and IFN-γ^+ trNKs (G) from the mice treated with itaconate/4-OI, which are reduced by IRG1-IN-1.

(H) ELISA revealing reduced IFN-γ level in renal tissues from the *Ncr1-iCre Acod1*$^{fl/fl}$ + HFD/STZ mice, compared with WT+HFD/STZ, *Acod1*$^{fl/fl}$ + HFD/STZ mice, an effect reversed by 4-OI treatment.

(I and J) Flow cytometry revealing reduced proportions of trNKs (I) and IFN-γ^+ trNKs (J) from the *Ncr1-iCre Acod1*$^{fl/fl}$ + HFD/STZ mice, compared with WT+HFD/STZ, *Acod1*$^{fl/fl}$ + HFD/STZ mice, an effect reversed by 4-OI treatment.

Data are presented as mean ± SD. Two-tailed unpaired Student's t test for (C and D), and two-way ANOVA with Tukey's post hoc test for (E-J). *p<0.05, **p<0.01, ***p<0.001.

221 **Graphical abstract**



222

Supplementary Files

This is a list of supplementary files associated with this preprint. Click to download.

- Graphicalabstract.pdf
- KeyResourceTable.docx
- SupplementalInformation.docx
- SupplementalInformation.docx